Applied Materials Today 16 (2019) 456–473

Contents lists available at ScienceDirect

Applied Materials Today

journal homepage: www.elsevier.com/locate/apmt

Radical-functionalized plasma polymers: Stable biomimetic interfaces for bone implant applications

Behnam Akhavan[a,b,c,*], Michiel Croes[d], Steven G. Wise[c,e], Chongpu Zhai[f], Juichien Hung[c], Callum Stewart[a], Mihail Ionescu[g], Harrie Weinans[d,h], Yixiang Gan[f], Saber Amin Yavari[d], Marcela M.M. Bilek[a,b,i,j]

[a] School of Physics, University of Sydney, Sydney, New South Wales 2006, Australia
[b] School of Aerospace, Mechanical, and Mechatronic Engineering, University of Sydney, Sydney, NSW 2006, Australia
[c] The Heart Research Institute, 7 Eliza Street, Newtown, Sydney, NSW 2042, Australia
[d] Department of Orthopedics, University Medical Center Utrecht, 3508 GA Utrecht, The Netherlands
[e] Sydney Medical School, Edward Ford Building (A27), Fisher Road, University of Sydney, NSW 2006, Australia
[f] School of Civil Engineering, University of Sydney, Sydney, Australia
[g] Australian Nuclear Science and Technology Organisation, New Illawarra Rd, Sydney, NSW 2234, Australia
[h] Department of Biomechanical Engineering, TU Delft, The Netherlands
[i] Charles Perkins Centre, University of Sydney, NSW 2006, Australia
[j] Sydney Nano Institute, University of Sydney, NSW 2006, Australia

ARTICLE INFO

Article history:
Received 10 April 2019
Received in revised form 10 July 2019
Accepted 15 July 2019

Keywords:
Bio-functional
Stability
Surface chemistry
Plasma polymerization
Bone implant
Osseointegration

ABSTRACT

Application of bio-functionalized coatings on bone implantable devices is a promising approach to direct rapid bone-implant integration. Plasma polymer (PP) films have become increasingly popular as platforms for surface bio-functionalization of implantable devices. However, the production of a reactive, yet stable PP film represents a technological challenge; as achieving a balance between the film's stability and functional group density is not trivial. Here we report the development of highly reactive and stable radical-functionalized PP films, using a combination of plasma polymerization and plasma immersion ion implantation. We provide new insights into the role of energetic ion bombardment on the growth mechanisms of plasma polymers by measuring the hydrogen content of PP structures using elastic recoil detection analysis. Nano-indentation and nano-scratch tests, as well as stability studies in simulated body fluid show a strong correlation between the degree of energetic ion bombardment and physico-chemical stability of the coatings. The potential of such ion-treated PP films to fabricate bio-functionalized implants that promote the functionality of primary osteoprogenitor cells is confirmed by studying cellular interactions after covalent attachment of fibronectin or bone morphogenetic protein (BMP)-2. We found that covalent attachment of fibronectin improved adhesion, spreading and proliferation of primary osteoblasts; whereas covalent attachment of BMP-2 enhanced the osteocalcin expression in bone-marrow isolated mesenchymal stem cells (MSC). These results present great promise for the fabrication of a new class of robust, biologically-functionalized interfaces for the surface engineering of biomaterials, particularly implants that need to be overgrown with bone-producing cells and thereby become firmly attached to host tissue.

1. Introduction

Rising incidences of osteoporosis-related bone fracture, bone cancer, and osteoarthritis-related joint replacement have resulted in an increasing number of orthopedic surgeries world-wide that require implants, which need firm bonding to bone [1]. A large number of these surgeries, however, fail due to poor bone integration or bacterial formation at the implant, leading to a high number of revision surgeries [2,3]. Patient discomfort, health risks, and economic burdens associated with revision surgeries provide a compelling need for strategies that facilitate rapid osseointegration around the implant surface [4,5]. Application of functional coatings on implantable devices is a viable approach to mitigate these problems by masking the implanted surfaces, mimicking the surrounding tissue, and allowing successful integration with the

* Corresponding author at: School of Physics, University of Sydney, New South Wales 2006, Australia.
E-mail address: behnam.akhavan@sydney.edu.au (B. Akhavan).

https://doi.org/10.1016/j.apmt.2019.07.002
2352-9407/

body [6,7]. Biologically functionalized surfaces, in particular, enable orthopedic implants to actively direct rapid implant-bone integration, thus reducing the need for revision surgeries [6,8,9].

Biofuntionalization of surfaces can be carried out through either physical adsorption or covalent immobilization of bioactive proteins. Physical adsorption is not a suitable immobilization approach; because the physisorbed proteins can be displaced by other molecules in the local biological medium in processes such as the Vroman effect [10]. A further major disadvantage of immobilization via physical forces is the accompanying protein denaturation that typically occurs and often reduces the biological activity of the immobilized molecules. Although covalent biofunctionalization through chemical linkers mitigates these problems, the chemistry involved in linker-mediated protein immobilization is often complex, substrate-dependent, and challenging to replicate consistently [11,12]. The large usage of solvents and chemicals in such wet-chemistry methods may also lead to problems in obtaining regulatory approval.

Plasma polymer (PP) thin films have become increasingly popular in recent decades for bio-functionalization of implants [13–15]. PP films are generally applied as interlayers to introduce chemically reactive groups onto biomaterial surfaces for subsequent conjugation of biological motifs such as proteins and peptides [16]. This solvent-free, versatile, and substrate-independent technique is suitable for the modification of virtually any solid material regardless of its shape, geometry, and chemistry. The physical and chemical properties of a PP film can, however, significantly change due to the interactions between the polymer coating and the environment [17]. The resistance of a PP film to such changes is referred to as 'stability' and presents crucial implications for almost any biological application. Examples of PP film instability upon insertion to an aqueous environment include oxidation of dangling bonds [18], leaching of low molecular weight species [19], swelling, and delamination from the substrate [20]. Degradable PP films are useful for particular applications, such as the release of drugs and other solubilized agents [21], but highly stable bio-interfaces are required for long-term cell adhesion and biomolecule immobilization [22].

Significant effort has been devoted to covalently immobilize bioactive molecules on PP interfaces through reactions with reactive chemical moieties, such as amine, carboxyl, and epoxy groups on the surface [16]. However, production of such chemically-functionalized PP films that present reactive functionalities as well as exhibiting long-term physical and chemical stability in biological environments has remained a central challenge for the field. Tuning the ratio of plasma input power to the precursor gas flow rate has typically been the focus of research to achieve stable PP interfaces [23–25]. Stability is enhanced by increasing plasma power, as it leads to increased cross-linking; but increasing plasma power typically fragments the required chemical moieties (Fig. 1a and b). Hence, we take an alternative approach to create plasma polymer films capable of direct attachment of biological molecules.

Our approach relies on a new version of plasma polymerization in which negative bias voltages are applied in a pulsed manner to the substrate during the film growth (Fig. 1c) [26–30]. This approach provides enhanced energetic ion bombardment during the film deposition, generating high concentrations of radicals embedded within the PP structure [31]. These long-living reactive radicals migrate to the surface and form covalent bonds with biomolecules in solution [32]. The bio-functionalization of interfaces through these PP interlayers does not, therefore, rely on the presence of specific chemical groups on the surface.

Here we present the development of highly reactive, yet stable PP films for use as biomimetic platforms for surface engineering of bone implantable devices. The requirements for interfacial robustness are particularly demanding for bone implant applications where significant abrasion or flexure occurs on surgical

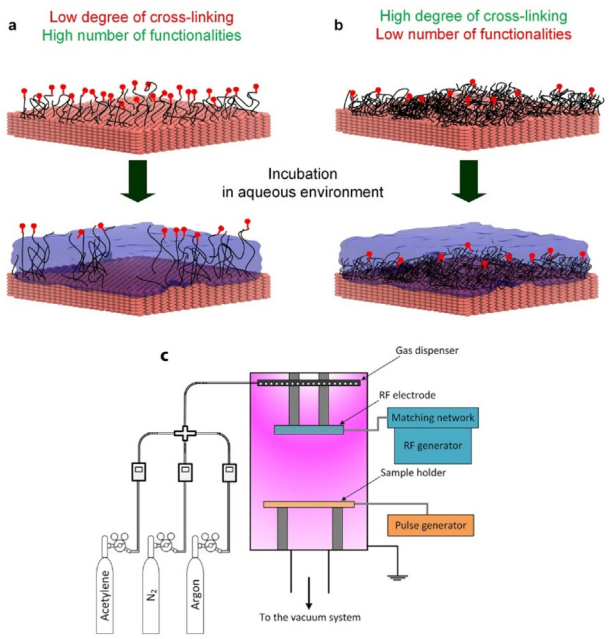

Fig. 1. The fabrication of chemically functionalized PP films represents a critical challenge, as preserving the chemical functionalities of the monomer is at the expense of physical stability in aqueous environments. (a) High concentrations of chemical functional groups (indicated as red circles) are retained in the PP film structure deposited at relatively low plasma energies, but the film is poorly cross-linked and shows low physical stability in the form of swelling or delamination after contact with aqueous media. (b) PP films deposited at relatively high plasma energies are sufficiently cross-linked and show desirable stability in aqueous environments, but limited number of chemical functional groups are retained in the polymer structure due to the increased fragmentation of the precursor monomer at high plasma energies. (c) Schematic illustration of the ion-assisted plasma polymerization system. The top electrode is connected to an RF power generator, while the substrate holder is negatively biased during the deposition.

insertion. The deposition of such ion-treated plasma polymers (IPP) at higher plasma energies not only enhances the film stability but also increases the concentration of functional sites, i.e. radicals, for covalent immobilization of biomolecules. This technology, therefore, allows for production of films with a combination of properties that could not be readily achieved using conventional plasma polymerization.

In this investigation, we shed light on the role of energetic ion bombardment in the growth mechanisms and physico-chemical stability of plasma polymer films. A mixture of acetylene, argon, and nitrogen gasses was used as the precursor monomer. We used acetylene as a model, simple carbon-containing monomer, as it is a low-cost, commercially available, and non-toxic gas. We demonstrate that with an optimum degree of ion bombardment, highly robust interfaces are produced for covalent immobilization of biologically potent molecules, such as fibronectin or bone morphogenetic protein (BMP)-2, thereby enhancing the functionality of bone producing cells that can firmly bind the implant to the host bone. Taken together, our results demonstrate that ion-assisted plasma polymerization is a promising approach for the development of a new generation of robust, radical-functionalized interfaces for surface engineering of bone implantable devices.

2. Experimental

2.1. Materials

Acetylene, argon, and nitrogen gasses were obtained from BOC Australia. Titanium foils were purchased from Firmetal, China and were used after sonication in toluene, acetone and, ethanol for

10 min following by drying using nitrogen blow. Sodium dodecyl sulfate (SDS), bovine serum albumin (BSA) and fibronectin from human plasma were obtained from Sigma-Aldrich. Bone morphogenetic protein (BMP)-2 was obtained from InductOS, Medtronic BioPharma B.V., Heerlen, The Netherlands.

2.2. Ion-assisted plasma polymerization

Ion-treated plasma polymer films were deposited on titanium and silicon substrates using a custom-made plasma polymerization system described before in detail [27,33,34]. The negative bias pulses had a constant frequency of 3 kHz with a pulse duration of 20 μs. A mixture of acetylene, argon, and nitrogen gasses were injected into the chamber at constant flow rates of 5, 10, and 15 standard cubic centimeters per minute (sccm), respectively; while the chamber working pressure was kept at 110 mTor. Base pressures were always kept below 5×10^{-2} mTorr. The substrates were initially cleaned with argon plasma (Ar flow rate = 40 sccm, RF power = 75 W, bias voltage = −500 V) for 10 min. Plasma polymer coatings were deposited for pulsed bias voltages varied from 0 to −1000 V at a constant RF power of 50 W. The plasma polymerization times were adjusted accordingly to obtain a constant thickness of approximately 40 nm for each deposition condition, unless otherwise stated.

2.3. X-ray photoelectron spectroscopy (XPS)

The surface chemistry of IPP coatings was examined using a FlexMode SPECS spectrometer equipped with a monochromatic Al Kα (hv = 1486.7 eV) radiation source, a hemispherical analyzer (PHOIBOS 150), and an MCD9 electron detector. The X-ray source was operating at 200 W (10 kV and 20 mA) at pressures below 5.0×10^{-8} mbar. The electron take-off angle was 90° with respect to the sample surface. The survey spectra were recorded at a pass energy of 30 eV and a resolution of 0.5 eV over the energy range of 0–1000 eV. The carbon (C 1s) and titanium (Ti 2p) high resolution spectra (0.1 eV) were obtained at a pass energy of 20 eV. The spectra were charge-corrected with reference to the binding energy of aliphatic carbon (284.6 eV). All XPS measurements were carried out within approximately 24 h after deposition, allowing a fixed aging time for all samples. C 1s and Ti 2p higher resolution spectra were curve fitted using a linear background, Gaussian (70%)–Lorentzian (30%) line shape, and equal full-width at half-maximum (FWHM) values. Survey spectra were used for elemental composition calculations. Curve fittings and elemental composition calculations were conducted using CasaXPS software, Version 2.3.14.

2.4. Time of flight secondary ion mass spectroscopy (ToF-SIMS)

ToF-SIMS data were collected using a PHI TRIFT V nanoTOF instrument (Physical Electronics, Chanhassen, MN) fitted with 30 eV $79Au^+$ pulsed liquid metal primary ion source (LMIG). The base pressure was always below 5×10^{-6} Pa, and the measurements were performed in positive SIMS mode. Dual charge compensation was achieved by employing an electron flood gun and Ar^+ ions at 10 eV. SIMS counts were recorded for at least six spots with areas of 100 μm × 100 μm per sample. WincadenceN software (version 1.8.1 provided by Physical Electronics) was used for spectra analyses.

2.5. Elastic recoil detection analysis (ERDA)

The hydrogen depth profile in IPP coatings deposited on silicon wafers was measured by ERDA with 2 MeV He ions. The samples were examined in a vacuum of 5×10^{-5} Pa, with the normal tilted 76° relative to the direction of the incident He ion beam. Recoiled hydrogen was measured with a solid-state detector placed at 28° scattering angle. In order to discriminate recoiled H from scattered He, a 9 μm thick Mylar filter was placed in front of the detector. All samples were bombarded with the same total number of He ions, reflected in the total charge of 3 μC accumulated for each measurement, providing a relative H content in the sample series.

2.6. Electron paramagnetic resonance (EPR) spectroscopy

The concentration of free radicals embedded into the structure of IPP coatings was evaluated using an EPR spectroscopy (Bruker EMXplus Xband). IPP-coated polystyrene films (7 cm × 7 cm), rolled into Wilmad Borosilicate glass NMR tubes were used for this analysis. Spectra were recorded with a central magnetic field of 3510 G, modulation amplitude of 3 G, microwave frequency of 9.8 GHz, and power of 25 Mw. The spectrometer was calibrated using a weak pitch sample. The field modulation frequency was 10^5 Hz. The sampling time was 85 ms, and 10 scans were averaged per sample.

2.7. Spectroscopic ellipsometry

The thickness and refractive index of the IPP coatings before and after incubation in SBF were measured using a Woolam spectroscopic ellipsometer. The high-speed monochromator (HS-190) and control module (VB-400) were operated by WVASE32 software. The system was initially calibrated using a standard silicon wafer. The spectra were collected for three angles of incidence (65°, 70°, and 75°) over the wavelength range of 200–1000 nm. A Cauchy model was utilized to fit the obtained data. The average values of at least three measurements per sample were reported as the film thickness and refractive index values.

2.8. Nano-indentation and nano-scratch measurements

The normal contact stiffness and scratch responses of IPP coatings deposited on titanium substrates were measured using an Agilent-G200 nano-indenter. Berkovich (Synton-MDP, XP/Berkovich/020) and conical (Synton-MDP, XP/Con060/005/020) tips were employed for nano-indentation and nano-scratch tests, respectively. The normal elastic responses of coatings were evaluated using partial unloading procedures in the nano-indentation tests [35,36]. After each unloading stage with the applied load decreasing by 20%, the loading level rose by a factor of two to the next unloading stage, until the load reached 50 mN corresponding to the last loading/unloading cycle. All the values of stiffness were determined by averaging over 20 tests at different positions on each sample. For nano-scratch tests, the conical tip proceeded at a velocity of 0.25 μm/s for a scratch distance of 200 μm within which the normal load increased linearly to 50 mN. Under the same experimental condition, ten scratches were made on each individual sample.

2.9. Atomic force microscopy (AFM)

Morphology and root-mean-square (RMS) roughness of IPP coatings deposited on silicon wafers were obtained by molecular imaging PicoSPM operating in noncontact AFM mode. The noncontact silicon tips (Nanosensors, PPP-NCST-SPL) had a frequency of 76–263 kHz. The scanner had a maximum range of 100 μm, and the samples were scanned at a set point of 2–3 V and a frequency of 0.5 Hz. The recorded data were processed using PicoScan 5 and WSxM software (Version 5.0, Nanotec Electronica).

2.10. Stability evaluation in simulated body fluid (SBF)

The chemical and physical stability of the IPP-coated Ti surfaces were evaluated by incubation in Tyrode's simulated body fluid (SBF) with a composition reported previously [34]. Samples were sterilized using ultraviolet (UV) light for 30 min prior to incubation for the durations of 7–60 days at 37 °C. The UV dose used for sterilization of samples is insignificant compared to the UV exposure inherent in the plasma treatment; and therefore it produced no further detectable physical or chemical changes. All samples were incubated in SBF within 24 h after deposition. The Tyrode's SBF was removed after incubation, and the samples were rinsed three times with Milli-Q water followed by drying with a stream of nitrogen gas. XPS spectra of the washed samples were obtained within 24 h.

2.11. Covalent immobilization of fibronectin

IPP-coated Ti surfaces were incubated overnight in fibronectin PBS solution with a concentration of 15 μg/mL at 4 °C except where stated otherwise. The samples were then thoroughly washed with PBS to remove excess unbound protein. To demonstrate the covalent immobilization of fibronectin, the samples were washed in 5% sodium dodecyl sulfate (SDS) for 15 min at 90 °C.

2.12. Covalent immobilization of BMP-2

For BMP-2 functionalization, uncoated and IPP-coated Ti foil or glass coverslips were incubated in 15 μg/ml BMP-2 dissolved in MilliQ water for 24 h at 4 °C in the dark. Non-functionalized samples were treated with MilliQ water in the same manner. Samples were washed three times with MilliQ water, air-dried overnight, and UV sterilized for 30 min prior to cell seeding. To demonstrate the strength of BMP-2 binding, samples were washed with 0.1% (v/v) Tween-20 (4 h at 37 °C) or 0.5% (w/v) sodium dodecyl sulfate (SDS, 1 h at 37 °C).

2.13. Enzyme-linked immunosorbent assay (ELISA)

ELISA was used to evaluate the attachment of fibronectin on surfaces. Fibronectin-coated surfaces were exposed to 5% BSA solution for 1 h and washed with PBS. A fibronectin rabbit-anti human primary (Ab2413, Abcam) was applied at a 1:5000 dilution (1 h) followed by a goat-anti-rabbit secondary antibody (ab6721) at a 1:20,000 dilution for 1 h. Bound antibody was visualized with incubation of samples in substrate solution 1-Step™ Ultra TMB (cat. 34028B, Thermofisher Scientific) for 30 min before 0.02 M sulphuric acid was added to stop the reaction. The absorbance of samples at 450 nm was measured with a plate reader.

2.14. Attenuated total reflectance (ATR) Fourier transform infrared (FT-IR) spectroscopy

The ATR FT-IR spectra of bare and IPP-coated Ti before and after incubation in the fibronectin solution were recorded using a Digilab FTS7000 FTIR equipped with an ATR accessory (Harrick, USA) with a trapezium germanium crystal (width = 1 cm) and an incident angle of 45°. Samples with a 2 cm × 1.5 cm area were used to fully cover the width of the ATR crystal. Each spectrum is the average of 500 scans recorded at a resolution of 4 cm^{-1}. Spectra of samples before protein immobilization were subtracted from those after the immobilization to reveal changes associated with the attached protein layer. The subtraction and analysis of spectra were performed using Resolutions Pro software (Digilab, V. 4.0).

2.15. Isolation and culture of primary osteoblasts from adult mouse long bones

Primary osteoblasts were harvested from (6–8)-week old C57BL/6 mice according to the standard protocol [37]. Male C57BL/6 were euthanized by cervical dislocation and sterilized with 70% ethanol for 5 min. Experiments were in accordance with the Australian Code of Practice for the Care and Use of Animals for Scientific Purposes. All personnel involved in the animal procedures have completed an approved animal care and ethics course. Hind limbs were exposed following a single incision through the dorsal skin and removed at the hip joint. Muscles, ligaments, and tendons were carefully disassociated from tibias and femurs which were then incubated in 2 mg collagenase II (Life Technologies) per ml in serum free Dulbecco's modified Eagle medium (DMEM) for 20 min at 37 °C ('digesting solution'). Bone marrow was flushed from the long bones with PBS, before cutting the diaphysis into 1–2 mm pieces, several washes in PBS and further incubation in 10 ml digesting solution for 2 h at 37 °C. Finally, bone chips were washed with growth medium (DMEM with 10% FBS, 100 μg/ml Penicillin, 100 μg/ml Streptomycin, 50 μg/ml ascorbic acid + 10 mM beta-glycerophosphate) three times for 5 min with 1200 rpm centrifugation. The washed bone chips were then placed in a 6-well plate with 3 ml growth medium. Within 5 days, osteoblasts were observed growing out of the bone chips. In 10–14 days, osteoblasts were ready to passage for further experimentation.

2.16. Osteoblast attachment, spreading, and proliferation

Primary osteoblasts (OB, passage 3–5) were used to study interactions with control titanium, titanium coated with IPP, and IPP titanium coated with fibronectin in 8-well chamber slides (ThermoFisher Scientific). For attachment studies, OBs (2×10^4 cells/well) were incubated with the surfaces for 1 h before washing with PBS and fixing with 70% ethanol for 10 min. Samples were washed twice with PBS, permeabilized with 0.05% Triton for 10 min and stained with ActinRed™ 555 for 10 min. Samples were mounted with 4′,6-diamidino-2-phenylindole (DAPI) fluoroshield mounting medium (Sigma Aldrich). Images from 4 fields, together covering the entire sample, were collected and cell nuclei counted using Image J. Cell area was also quantified to determine spreading. For proliferation, OBs (4×10^3 cells/well) were incubated for 3, 6, 10 and 14 days, with media changed every second day, and metabolic activity measured using the MTS cell proliferation assay kit (Promega). The MTS reagent (40 μl per well) was added to each well and was further incubated for 2 h. The formazan dye produced by viable cells was quantified by measuring the absorbance at 490 nm.

2.17. BMP-2 bioactivity using ATDC5 reporter cells

BMP-2 bioactivity was assessed with the ATDC5 cell line (ATCC, Manassas, VA, USA), as these cells are known to rapidly produce the bone apposition marker alkaline phosphatase (ALP) in presence of BMP-2 [38]. Cells were seeded onto the surfaces at an initial density of 10,000 cells/cm^2 in solution consisting of DMEM/F12 medium (Gibco, Grand Island, NY, USA) supplemented with 10% FBS and 100 units/mL penicillin/streptomycin (Invitrogen, Carlsbad, CA, USA). ALP activity was measured in cells cultured on Ti surfaces for 72 h, by conversion of the p-nitrophenyl phosphate liquid substrate system (Sigma), after permeabilization in 0.2% (v/v) triton X-100/PBS for 15 min. The absorbance was measured at 405 nm and corrected at 655 nm (Bio-Rad, Hercules, CA, USA). The ALP value of each sample was normalized to its DNA content, measured with the Quant-It PicoGreen kit (Invitrogen), according to

the manufacturer's instructions. For qualitative assessment of ALP activity, ATDC5 cells were cultured on glass coverslips for 72 h. Cells were fixed in 4% (w/v) formaldehyde for 10 min, permeabilized in 0.2% (v/v) triton X-100 in PBS for 15 min, and stained using the Fuchsin+ Substrate-Chromogen kit (Agilent), according to the manufacturer's instructions.

2.18. Human mesenchymal stem cell (MSC) biocompatibility and osteogenic differentiation

Bone marrow was obtained from the calcaneus bone of an adolescent female undergoing orthopedic surgery (University Medical Center Utrecht, Utrecht, The Netherlands) after written informed consent and approval of the local medical ethical committee. The mononuclear cell fraction was isolated by Ficoll-Paque centrifugation. Plastic-adherent cells within this fraction were expanded to passage 5 in MSC growth medium, consisting of α-MEM (Invitrogen, Carlsbad, CA, USA) medium with 10% (v/v) FBS, 100 units/mL penicillin/streptomycin (Invitrogen), and 0.2 mM l-ascorbic acid 2-phosphate (Sigma, St. Louis, MO, USA). The multipotency and expression of surface antigens of these MSCs were described before [39], and are in accordance with the minimal criteria of human MSCs according to the International Society for Cellular Therapy [40]. In all MSC experiments, cells were seeded at an initial density of 7500 cells/cm^2 on Ti foils in MSC growth medium.

MSC metabolic activity was measured every day until day 5 using the alamarBlue Cell Viability Reagent (Thermo Fischer, Waltham, MA, USA). Fluorescence was detected utilizing the Fluoroskan Ascent FL multiplate reader (Thermo Labsystems, Helsinki, Finland) after 1 h incubation with alamarBlue reagent. Cell viability and proliferation were assessed qualitatively using a live/dead cell viability kit, as described by the manufacturer (Molecular Probes, Thermo Scientific). Live (green) and dead cells (red) were imaged using a fluorescence microscope (IX53, Olympus, Tokyo, Japan).

The osteocalcin expression was assessed as a marker of MSC osteogenic differentiation, since it is a bone-specific protein synthesized by osteoblasts [41]. Cells were cultured for 14 days, with the medium being refreshed every fourth day. The cell monolayers were fixed for 15 min in 80% (v/v) methanol and permeabilized for 10 min with 0.2% (v/v) Triton X-100/PBS. After a blocking step of 30 min with 5% (v/v) bovine serum albumin (BSA)/PBS, samples were incubated for 1 h at room temperature with 10 μg/mL mouse monoclonal antibody recognizing human osteocalcin (clone OCG4, Enzo Life Sciences, Farmingdale, NY). This was followed by incubation with 10 μg/mL goat-anti-mouse polyclonal antibody conjugated to Alexa Fluor 488 (Invitrogen). Counterstains for DAPI (4′,6-diamidino-2-phenylindole, 1 μg/mL for 10 min) and phalloidin-TRITC (2.5 μg/mL for 30 min) were performed to demonstrate the cell nuclei and cytoskeleton, respectively. Cells were imaged using a fluorescence microscope (IX53, Olympus, Tokyo, Japan). Osteocalcin staining was quantified in ImageJ freeware version 1.48 (U.S. National Institutes of Health) on binary images after applying a global threshold. The average count was determined for six images (total surface area 3 mm^2) obtained from an experiment run in triplicate. The day 14 osteocalcin count was normalized to the day 14 DNA content (Quant-It PicoGreen kit) determined in a parallel experiment performed under the same conditions.

2.19. Statistical analyses

The data, expressed as mean ± SEM (standard error of the mean), were compared using GraphPad Prism version 7.02 (Graphpad Software, San Diego, California) for PC. One-way and two-way ANOVA with a Tukey's multiple comparisons post-test were conducted to compare between groups and within groups respectively. Statistical significance is indicated in figures as $^*p < 0.05$, $^{**}p < 0.01$ and $^{***}p < 0.001$.

3. Results and discussion

3.1. Deposition of ion-treated plasma polymer (IPP) films

3.1.1. Surface chemistry

In most plasma polymerization systems, film-forming species do not possess sufficient energy to form chemical bonds with the substrate material unless there is a high flux of ionized species arriving at the surface [42]. Here we employ a unique configuration of plasma polymerization to enhance the plasma-substrate interaction during the film deposition. In this arrangement, we employ two sources of plasma power: (i) a radio frequency source for exciting the precursor gas into the plasma state, and (ii) a pulsed negative bias voltage source connected to the substrate. Applying a negative bias to the substrate enhances the bombardment of accelerated positive ions during the plasma polymer film growth. This combination of plasma polymerization and ion implantation is expected to be beneficial in two respects: First, it results in a high concentration of radicals embedded within the IPP film structure; and second, it yields strong interaction between the deposited species and the substrate at early stages of film growth. We evaluated this hypothesis by the deposition of IPP films at bias voltages ranging from 0 to −1000 V, while the plasma energy from the RF source was kept constant at 0.1 kJ cm^{-3}.

Fig. 2a shows XPS survey elemental composition of IPP films as a function of pulsed bias voltage (V_b). By increasing the bias voltage from 0 to −1000 V, the atomic concentration of carbon increases from 67 to 75%, while that of nitrogen decreases from 25 to 13%. Although no oxygen is present in the precursor gas mixture ($Ar + C_2H_2 + N_2$), between 8 to 12% oxygen was observed on the surfaces with an increasing trend as a function of bias voltage. The incorporation of oxygen into the IPP film structure is either due to post-deposition oxidation in atmosphere or plasma phase contamination associated with residual oxygen in the deposition chamber. Considering the relatively low base pressure of the deposition chamber ($<5.0 \times 10^{-5}$ Torr), the former appears to be the dominant source of detected oxygen. The post deposition oxidation of plasma polymerized films is an inevitable process that has also been reported for other precursor monomers [43,44]. The increase of oxygen on the surface as bias voltage increases is explained by greater ion bombardment of the growing film at higher bias voltages, resulting in the generation of a higher concentration of radicals susceptible for post-deposition oxidation [45,46].

To further elucidate the role of enhanced ion bombardment on the surface chemistry of IPP films, we curve-fitted the C 1s high resolution spectra as shown in Fig. 2b. Three peaks associated with C–C/C–H at binding energy (BE) ≅ 284.6 eV, C–O/C–N at BE ≅ 286.5 eV, and C=O/N–C=O at BE ≅ 287.5 eV.38,42 were fitted in the C 1s high resolution spectra. By increasing the applied bias, the C 1s peak becomes progressively more asymmetric and the shoulder at higher binding energies becomes narrower. As the bias voltage increases, there is an increase in the concentration of carbon compounds in the neutral environment and a decrease in oxygen- and/or nitrogen-containing moieties. The increase of oxygen atomic concentration as a function of bias voltage (Fig. 2a) indicates that the reduced concentration of components at higher binding energies is primarily due to the decrease of nitrogen-containing moieties. Such changes are also in agreement with the reduction of nitrogen atomic concentration as a function of bias voltage (Fig. 2a). Further evidence for the depletion of nitrogen-containing species at higher bias voltages is obtained by ToF-SIMS normalized positive counts shown in Fig. 2c.

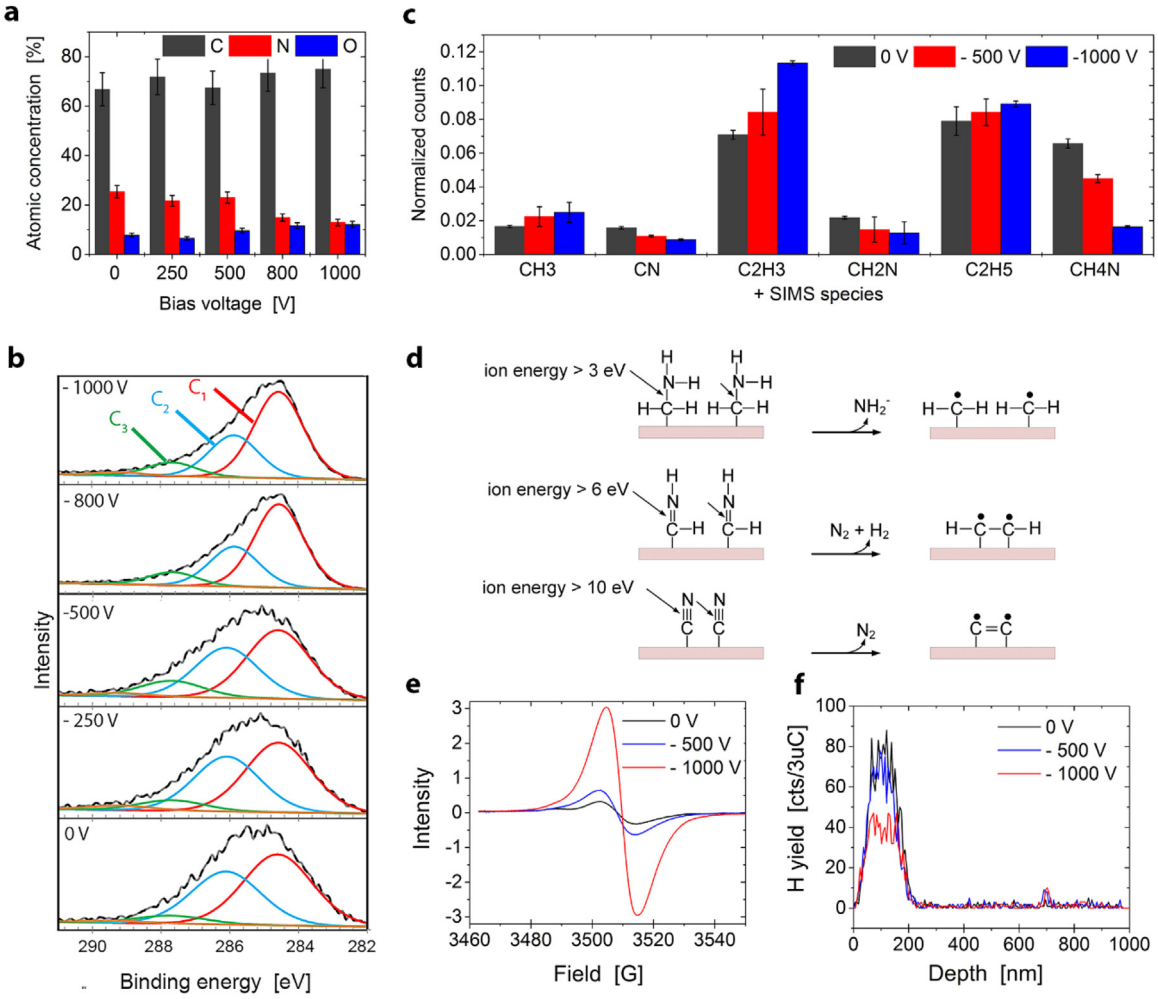

Fig. 2. Chemical characterization of IPP films. (a) XPS survey elemental composition of the films as a function of applied bias voltage. (b) C 1s high-resolution spectra of the films deposited at various applied bias voltages. The spectra are curve-fitted by three components: C_1: C–C/C–H, C_2: C–O/C–N, and C_3: C=O/N–C=O. (c) Average normalized positive SIMS counts of carbon/nitrogen-containing species from ToF-SIMS for the films deposited at $V_b = 0$, −500, and −1000 V. (d) Suggested mechanism of nitrogen depletion due to energetic ion bombardment resulting in the formation of carbon-centered radicals. (e) EPR spectra of PP films deposited at $V_b = 0$, −500, and −1000 V. The broad and symmetrical peaks are indicative of unpaired electrons that are associated with radicals. (f) ERDA hydrogen yield profiles obtained for PP films deposited at varied bias voltages.

Increasing the V_{bias} from 0 to −1000 V results in a significant increase of hydrocarbon counts, (CH_3, C_2H_3, and C_2H_5) and a decrease in nitrogen-containing fragments (CN, CH_2N, CH_4N).

We describe this decrease of nitrogen atomic concentration by an etching mechanism that selectively ablates the nitrogen-containing species under enhanced ion bombardment conditions. This preferential etching mechanism can be explained by high electron density of nitrogen and sp/sp^2 hybridized carbon in chemical groups such as –C=N, N–C=O, and –C≡N [47]. Atoms with higher electron densities demonstrate a greater reactivity with positive ions arriving at the surface, and thus can be more easily ablated from the film structure. As indicated by ATR FT-IR data (see Fig. S1 in Supporting Information), single, double, and triple bonds in carbon-nitrogen containing species are formed by the plasma polymerization of acetylene and nitrogen. It is, therefore, plausible to suggest that at lower bias voltages, mainly C–N bonds with a relatively low dissociation energy (305 kJ mol^{-1}) are broken. In contrast, at higher bias voltages, ions with greater energies are capable of breaking C=N (615 kJ mol^{-1}) and C≡N (891 kJ mol^{-1}) bonds as well. This suggested mechanism of nitrogen depletion that results in the formation of carbon-centered radicals is illustrated in Fig. 2d. The higher mobility of atoms at elevated ion-bombardment conditions may also facilitate the diffusion of liberated nitrogen atoms. Diffusion allows the liberated atoms to form volatile species in combination with other similarly liberated species, move to the surface and be evacuated from the plasma chamber.

A radical has an unpaired electron and an associated electron spin. Electron paramagnetic resonance (EPR) spectroscopy can directly measure the density of electron spins, i.e. the concentration of radicals. EPR spectra of the films deposited with applied bias voltages of 0, −500, and −1000 V are shown in Fig. 2e. The EPR spectra are broad, approximately symmetrical, and show single resonance peaks. The resonance peaks are centered at 3513 G (g-value of 2.003) and are assigned to unpaired electrons associated with radical-containing compounds within the IPP structure. Double integration of EPR spectra and comparison with a standard pitch sample reveals a radical concentration of $\sim 1.6 \times 10^{17}$ spins cm^{-3} for the plasma polymer film prepared at $V_b = 0$. This value agrees with a recent report on methane PP films deposited on substrates at floating potentials [48]. During the plasma polymerization process, the growing film is continuously bombarded by electrons, photons, and positively charged ions generated in the plasma phase [49]. Such interaction between the plasma polymer film and the plasma phase yields surface radicals that can be trapped within the film structure. By the application of pulsed biases of −500 and −1000 V, the concentration of radicals increases to $\sim 5.1 \times 10^{17}$ and

$\sim 1.8 \times 10^{18}$ spins cm^{-3}, respectively. These data indicate that the ion-assisted plasma polymerization, achieved through pulse biasing a substrate, yields markedly larger concentrations of radicals compared to conventional plasma polymer films deposited either on grounded or self-biased substrates. Higher substrate bias voltages result in higher degrees of energetic ion bombardment that in turn increase the likelihood of hydrocarbon fragmentation, chain scission, and bond cleavage; yielding greater concentrations of radicals within the growing film. These results are also in agreement with the mechanism we proposed for the formation of carbon-centered radicals due to the depletion of nitrogen atoms under enhanced ion bombardment conditions (Fig. 2d). It has previously been demonstrated that such reactive radicals are mobile and migrate from reservoirs beneath to the surface where they form covalent bonds with biomolecules [32].

The evaluation of hydrogen content of IPP structures not only sheds light on the mechanisms of plasma polymerization but also provides useful information on the role of hydrogen in the chemical stability of the coatings. However, measuring the hydrogen content is not straight-forward, because hydrogen has no core electrons and is not detectable by XPS [50]. We measured the concentration of hydrogen by elastic recoil detection analysis (ERDA) using He ions. Such data are significantly valuable as very limited knowledge on the variations of hydrogen content in plasma polymerized films is available in the literature due to experimental difficulties. Fig. 2f shows the relative ERDA hydrogen yield profiles obtained for IPP films deposited on silicon wafers at varied bias voltages. The deposition time was adjusted accordingly to obtain a constant film thickness of 180 nm for these measurements. From the profiles, it is evident that hydrogen is present predominantly up to a depth equivalent to the thickness of the films, and almost no hydrogen is detected in the silicon substrate. The average hydrogen yield within the depths of 50–150 nm are 68.11, 60.88, and 39.16 Cts/3 μC for PP films deposited at bias voltages of 0, −500, and −1000 V, respectively. Only the bulk of the films were considered for averaging in order to discount the influence of IPP film interfaces with air or the substrate on the measured values. These results manifest a significant depletion of hydrogen atoms for the film deposited at $V_b = -1000$ V compared to $V_b = 0$ and −500 V.

Such reduction of hydrogen content by increases in negative bias voltage is in agreement with previously reported ERDA measurements for carbon films deposited by RF plasma deposition of methane, where a greater removal of weakly bonded hydrogen was observed for higher negative bias voltages [51]. We suggest a hydrogen loss mechanism for the depletion of hydrogen atoms at high substrate bias voltages. Under intense energetic ion bombardment conditions, a great concentration of hydrogen radicals is formed due to the enhanced cleavage of molecular bonds in the tracks of impinging ions; a hypothesis that is also supported by the ESR data (Fig. 2e). Thus, it is highly possible that a significant portion of these hydrogen radicals recombine and eventually escape from the structure in the form of H_2, leaving behind a plasma polymer structure with a lower concentration of hydrogen atoms.

Table 1
XPS survey elemental composition and area percentage of components present in Ti 2p high resolution spectra for interfaces between titanium surfaces and IPP films (thicknesses ≅ 5 nm) prepared at various bias voltages.

Bias voltage (V)	Atomic concentration (%)				% Area of Ti 2p		
	C	N	O	Ti	TiO_2	TiO_x	Ti–Ti/Ti–C
0	65.8	14.8	14.5	4.9	90	2.7	7.3
−500	66.4	15.4	13.9	4.3	78.5	7.9	13.6
−1000	63.4	12.6	19.4	4.6	80.6	5.9	13.5

3.1.2. *Interface chemistry*

Analyzing the chemistry of IPP coatings at the interface of the titanium substrate provides valuable information about the role of ion bombardment on chemical interactions between the depositing polymer species and the substrate. To obtain information from initial stages of film growth, we deposited films with thicknesses of approximately 5 nm that are less than the sampling depth of XPS which is 8–10 nm. This strategy allows recording of XPS signals originating from both the IPP coating and the titanium substrate. The XPS survey spectra of these ultra-thin films showed titanium peaks with atomic concentrations of 4–5% (Fig. 3a, Table 1), confirming that the XPS signals originated from the IPP film-substrate interface. XPS C 1s and Ti 2p high-resolution spectra from IPP coating-substrate interface are shown in Fig. 3b and c, respectively. The C 1s high-resolution spectrum of the interface created without the application of substrate bias ($V_{bias} = 0$ V) consists of C–C/C–H, C–O/C–N, and C=O/N–C=O compounds. However, the C 1s spectra from interfaces created under ion-assisted plasma polymerization ($V_b = -500$ and −1000 V) exhibit a more complex structure. Apart from the organic carbon-containing moieties, two additional components, observed at binding energies of ∼282.5 and ∼289.8 eV, can be assigned to metallic carbide (TiC) and

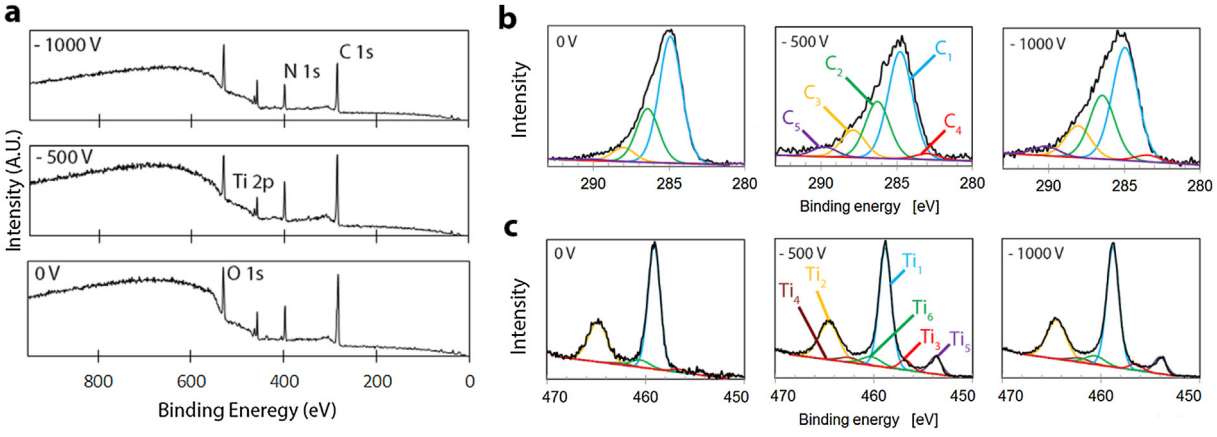

Fig. 3. Chemical characterization of interfaces between IPP films and titanium surfaces. (a) XPS survey spectra of thin IPP films (thicknesses ≅ 5 nm) deposited on titanium surfaces using bias voltages of 0, −500 and −1000 V. (b) XPS C 1s high-resolution spectra of thin IPP films deposited on titanium surfaces. The spectra are curve-fitted by five carbon-containing components: C_1: C–C/C–H, C_2: C–O/C–N, C_3: C=O/N–C=O, C_4: TiC, and C_5: titanium oxycarbides. (c) XPS Ti 2p high-resolution spectra of thin IPP films. The spectra are curve-fitted by six titanium-containing components: Ti_1: $(TiO_2)_{3/2}$, Ti_2: $(TiO_2)_{1/2}$, Ti_3: $(TiO_x)_{3/2}$, Ti_4: $(TiO_x)_{1/2}$, Ti_5: (Ti–Ti/Ti–C)$_{3/2}$, and Ti_6: (Ti–Ti/Ti–C)$_{1/2}$.

oxycarbide (TiO_xC_y) species, respectively [52,53]. The formation of these carbon-containing compounds is in agreement with the information obtained from Ti 2p high resolution spectra (Fig. 3c). The Ti 2p is a doublet due to the spin–orbit splitting of Ti $2p_{3/2}$ and Ti $2p_{1/2}$ with a separation energy of 5.7 eV [$\Delta E = E(Ti\ 2p_{1/2}) - E(Ti\ 2p_{3/2})$]. Ti $2p_{3/2}$ peaks for titanium in a neutral environment (Ti–Ti, Ti–C), titanium sub-oxides (TiO_x with $0 < x < 2$), and TiO_2, were fitted at BEs of, 456.4–457.0, 453.8–454.6, and 458.8–459.2 eV, respectively [52–54]. The area percentage of Ti–Ti/Ti–C compounds calculated from these spectra (Table 1) increase from 7.3% for the film prepared at $V_b = 0$ to 13.6% and 13.5% for the films deposited at $V_b = -500$ and -1000 V, respectively. Considering that the titanium atomic concentration was similar for these three samples (4–5%), this increase in area percentage must be attributed to the formation of Ti–C bonds. Titanium is an early transition metal with excellent propensity to form stable carbide bonds with a formation enthalpy of $-184.10\ kJ\ mol^{-1}$ [55]. XPS results imply that energetic ions arriving on a biased substrate provide sufficient energy to enter the substrate and form such chemical bonds between the arriving species and the substrate. The formation of metallic carbon-containing species at $V_b \geq -500$ V and the absence of these compounds for $V_b = 0$ V highlights the critical role of ion bombardment on regulating the growth mechanisms of plasma polymer films. The formation of chemical bonds between the first layers of IPP films and the substrate has significant implications for the improvement of film adhesion to the substrate, as discussed in the following sections.

3.1.3. Surface physico-mechanical properties

The thicknesses of IPP films obtained by spectroscopy ellipsometry were used to calculate deposition rates plotted as a function of bias voltage in Fig. 4a. The deposition rate is remarkably higher for $V_b = 0$ and -250 V than $V_b \geq -500$ V. This behavior implies that the ion-assisted plasma polymerization is controlled by a competitive polymerization and ablation process regulated by the arrival of energetic ions at the surface. The higher deposition rates at lower V_b values indicate that the polymerization process is predominant; whereas the reduction of deposition rate at $V_b \geq -500$ V suggests that the balance of polymerization and ablation processes tends more toward the ablation at higher V_b values.

The deposited energy density (ε) during the film growth is quantified as ion energies per deposited atoms and is obtained by [56,57]:

$$\varepsilon = \frac{\Gamma_i E_i}{R} \quad (1)$$

where Γ_i, E_i, and R are the ion flux incident on the substrate, the average energy of ions arriving at the substrate, and the deposition rate, respectively. The energy density during the film formation is enhanced by an increase in the average energy of ions (as at higher bias voltages) as well as a decrease in the deposition rate. At greater V_b values, higher ion flux (Γ_i) and energy (E_i) together with lower deposition rates (R) yield higher energy densities resulting in enhanced ion-assisted ablation. This explanation is further supported by the AFM topography images shown in Fig. 4b. The IPP film deposited at the bias voltage of -1000 V manifests distinct surface morphologies compared to those prepared at $V_b = 0$ and–500 V. It is observed that upon application a -1000 V bias voltage, crater-like features with peak-to-valley depths of 2–4 nm form on the surface. It appears that these features originate from an intense energetic particle bombardment, resulting in the ablation of the deposited films.

The variations in the cross-linking degree of the IPP films can be inferred from the changes in refractive index values plotted as a function of applied bias in Fig. 4c. The trend of changes in the refractive index follows that of variations in the deposition rate (Fig. 4a). By initial increases of the applied bias from 0 to 250 V, the refractive index remains almost constant at ~1.63, whilst it increases to 1.81 ± 0.01 by further increasing the bias voltage to -1000 V. The refractive index of a polymer is indicative of its degree of cross-linking and density [58]. The higher refractive indices measured for the IPP films deposited at $V_b > 250$ V is explained by higher fluxes of energetic ions arriving at the surface and thus greater fragmentation of deposited species. The recombination of fragmented species is facilitated through higher concentration of available radical sites, yielding highly cross-linked structures. This explanation correlates well with EPR data (Fig. 2e) that showed significantly higher concentrations of radicals formed at higher bias voltages and the removal of hydrogen atoms as shown by ERDA data (Fig. 2f).

The stability of plasma polymer coatings in aqueous media is attributed, in part, to their mechanical properties, e.g. elasticity and stiffness as well as their average residual stress. We performed nano-indentation to evaluate the influence of ion treatment on the Young's modulus of the coatings with thicknesses of approximately 100 ± 10 nm. The modulus of elasticity (E) as a function of indentation depth for uncoated and PP-coated titanium surfaces are shown in Fig. 4d. The modulus of elasticity for the uncoated titanium surface decreases from ~153 GPa for an indentation depth of 11.0 ± 1.9 nm to approximately 122 GPa for indentation depths greater than 60 nm. The higher E values measured at indentation depths <60 nm are due to a stiff native oxide layer with a thickness of a few nanometers naturally present on titanium surfaces [59]. The variations of E for IPP-coated surfaces, however, exhibit an opposite trend compared to that for the uncoated titanium. The E values for the coated samples increase as the indentation deepens to about 100 nm and remain approximately constant at 108 GPa by further increases in the indentation depth. Most importantly, for shallow indentation depths, where the influence of the substrate is minimal, significantly lower Young's moduli are measured for the film deposited at $V_b = 0$ V in comparison with those deposited at $V_b = -500$ and -1000 V. These results are consistent with the higher refractive indices measured for the IPP coating prepared at greater applied bias voltages (Fig. 4c), and suggest that the mechanical stiffness of this coating is elevated due to increases in the cross-linking density and consequent reductions in polymer chain flexibility.

The residual compressive stress of the films was evaluated by measuring the radii of curvature of silicon wafers before and after the deposition of the films. The profiles of IPP-coated silicon substrates prepared at various applied bias voltages are measured using stylus profilometry and shown in Fig. 4e. The increase in the deflection at the center of the profile after the deposition of PP coatings is a measure of the compressive residual stress. The residual stresses calculated from these profiles are 0.12, 0.20, and 0.52 GPa for the coatings deposited at $V_b = 0$, -500, and -1000 V, respectively. This increase of residual stress as a function of applied bias voltage is explained by densification of the coatings as confirmed by increases in the refractive index (Fig. 4c). [60] A highly cross-linked structure, formed under energetic ion bombardment conditions, results in the restricted mobility of polymeric chains that in turn hinders the release of stresses induced during the deposition.

Ramp load nano-scratch tests data provide further knowledge on mechanical properties of coatings deposited by ion-assisted plasma polymerization. The nano-scratch tests were performed over a length of 200 μm, while the normal load was increased linearly with the scratch distance. Fig. 4f shows representative scratch test results together with their corresponding post-scratch optical microscopy images. The normal load at which the film delaminates from the substrate is referred to as the 'critical load' (CL). The CL can be verified as a force corresponding to the delamination point in post-scratch images and associated discontinuity and fluctuation occurring in the lateral force-distance curve [61–65]. The greatest critical load of 33.2 ± 9.08 mN is achieved for the coating deposited

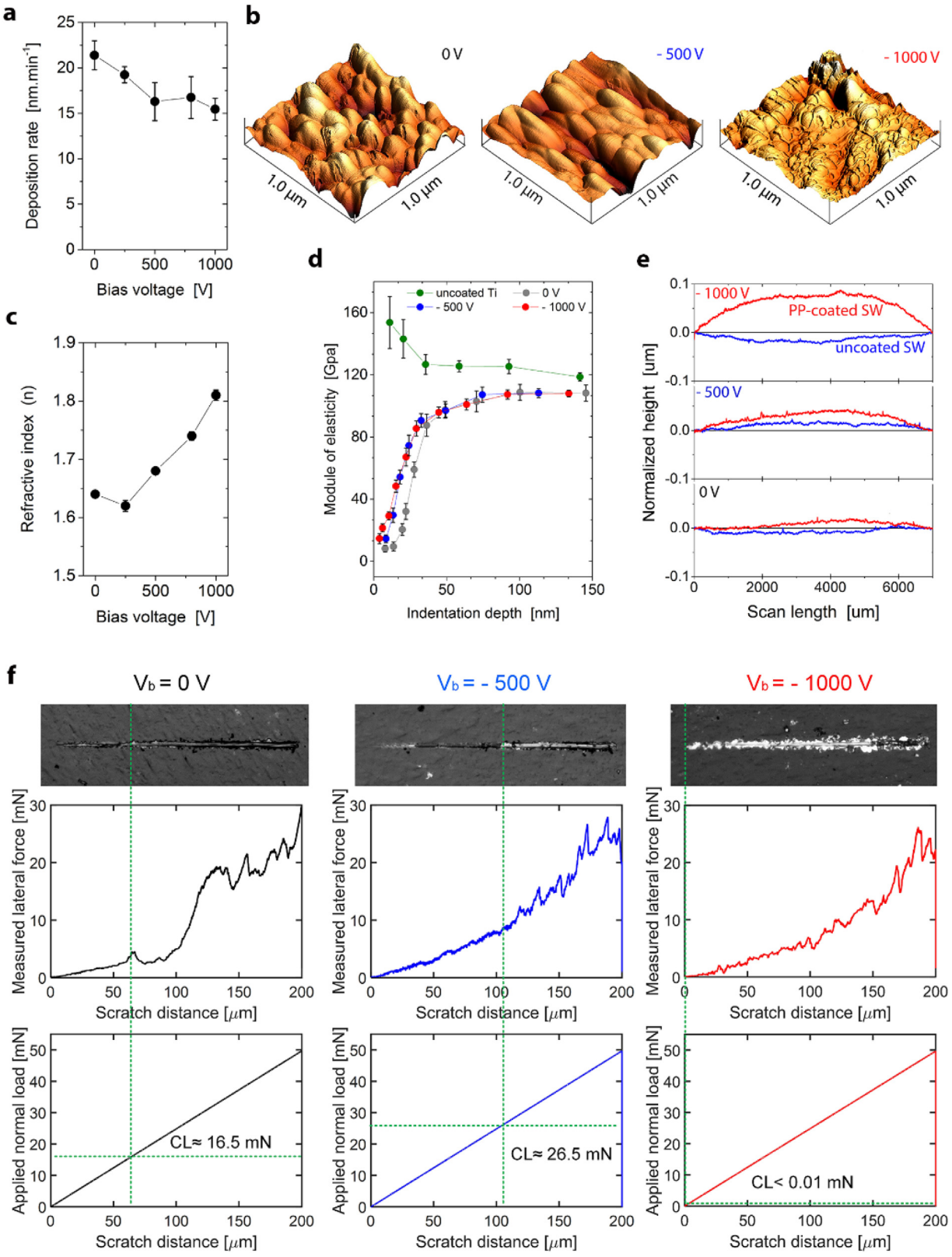

Fig. 4. Physico-mechanical characterization of IPP films. (a) Deposition rate of PP films as a function substrate bias voltage. (b) AFM images of IPP films deposited on polished titanium substrates at various bias voltages. The Z height is 18 ± 1 nm. (c) Refractive index (at λ = 630 nm) of PP films as a function of bias voltage. (d) Modulus of elasticity as a function of the indentation depth measured by nano-indentation on uncoated titanium and PP films deposited on titanium with various bias voltages. (e) The profiles of PP-coated silicon substrates prepared at various applied bias voltages. (f) Representative scratch test results together with their corresponding post-scratch optical microscopy images. The lateral load at which the film delaminates from the substrate is indicated as critical load (CL).

at $V_b = -500$ V, whilst the coating deposited without applying a bias voltage shows a significantly lower CL of 12.3 ± 5.51 mN. As observed from the post-scratch optical profile, the delamination of the film deposited at the maximum bias voltage ($V_b = -1000$ V) occurs within the first few micrometers of the scratch line with a CL of less than 4 mN. The CL of coatings deposited at $V_b = 0$ and -500 V is indicative of the film-substrate adhesion strength, since the penetration depth at the delamination point was markedly larger than the thickness of the films. The greater CL for the film deposited at $V_b = -500$ V compared to that for $V_b = 0$ verifies that ion-assisted plasma polymerization yields superior interfacial adhesion strength in comparison with conventional plasma polymerization where no external bias voltage is applied. These results, together with XPS data (Fig. 3b and c), confirm that the strong adhesion to the substrate achieved for $V_b = -500$ is associated with the formation of metallic carbide and oxycarbide bonds at the film-substrate interface. For the film deposited at $V_b = -1000$ V, however, the early stage delamination implies that the failure is cohesive rather than adhesive. This hypothesis is consistent with high compressive residual stress and high modulus of elasticity measured for this coating. These results indicate that breakdown of intermolecular bonding in such a 'stiff' structure surpasses the failure of the coating-substrate interface. The cohesive failure of this film is also in agreement with the robust interface formed under such elevated energetic ion bombardment conditions; a hypothesis that is supported by the formation of carbide/oxycarbide compounds during the initial stages of deposition.

3.2. Stability of ion-treated PP films in simulated body fluid

3.2.1. Chemical stability

Plasma polymerized films are susceptible to oxidation upon exposure to atmosphere, and nitrogen-rich films are prone to loss of nitrogen-containing groups in aqueous environments [66]. The oxidation of a plasma polymer film not only changes the surface chemistry but also results in detrimental consequences for the film integrity [67]. The degradation rate of polymeric films in aqueous media depends on the diffusion rate of oxygen and water molecules throughout the film thickness as well as the reactivity of metastable compounds produced during the initial stages of oxygen uptake [49]. Studies on stability should, therefore, be performed for extended durations of incubation in aqueous media to ensure sufficient progression of both diffusion and reaction-limited processes. This has been overlooked in the literature, and a large number of studies on plasma polymer films stability have applied incubation times of less than 24 h [19,68–70]. To evaluate the stability of IPP films in biological media, we incubated the samples in Tyrode's simulated body fluid (SBF)[71,72] at 37 °C for durations of up to 2 months.

Fig. 5a shows the XPS elemental compositions of IPP-coated titanium surfaces as a function of applied bias voltage before and after incubation in the SBF solution. The carbon atomic concentration does not significantly vary for various incubation times. By increasing the incubation time, the oxygen atomic concentration increases; while that of nitrogen decreases. Such changes in surface chemistry can primarily be attributed to a chain of auto-oxidation reactions initiated at abundantly available carbon-centered radicals at the surface (see Fig. 2e). The suggested possible oxidation pathways initiated from a carbon-centered radical are depicted in Fig. 5b. In this process, dissolved oxygen atoms initially oxidize the reactive radicals into metastable species such as peroxy radicals (C–O–O·) that are subsequently oxidized to more stable compounds containing carbonyl and carboxyl groups [18,25]. The loss of nitrogen can be attributed to the out-diffusion of volatile N-containing compounds, such as NH_3, that could have been trapped within the polymer structure. Additional oxidation reactions may also initiate from nitrogen-containing groups. For example, it is possible that hydrogen abstraction from N–H bonds contributes in the oxidation process, as previously suggested by Gengenbach et al. [73] Hydrolysis reactions are another important source of the oxygen uptake and the loss of nitrogen. Such reactions may involve O-R primary species present in the plasma polymer structure as well as secondary compounds, such as esters, produced by the oxidation reactions. Hydrolysis reactions may result in the loss of nitrogen through leaching of nitrogen-containing degradation products, such as ammonia, as in the case for amino-containing hydrocarbon plasma polymer films [66].

The changes in surface elemental composition as a function of applied bias voltage indicate the crucial role of ion treatment on the oxidation behavior of the films. From Fig. 5a, it is observed that the films deposited at bias voltages of 0 and -250 V show a higher uptake of oxygen and further reduction of nitrogen after incubation compared to those deposited at greater applied bias voltages. The comparison of XPS C 1s high resolution spectra of the films after 2 months incubation further highlights the role of ion-treatment on the chemical stability (Fig. 5c). Calculated atomic concentrations of various carbon-containing groups are plotted in Fig. 5d. These data show that minimal changes in the concentration of C=O, N–C=O groups are observed for the sample prepared at $V_b = -1000$ V and -500 V, whereas substantial increases in the concentration of these groups are observed upon incubation of the film deposited at $V_b = 0$ V.

The greater chemical stability of IPP films deposited at higher bias voltages may appear to be in contrast to the commonly accepted view that plasma polymer films containing higher concentrations of radicals suffer from a greater degree of oxidation and hydrolysis [25,49,73]. Although the greater initial density of trapped radicals is expected to yield higher oxidation rates, we suggest that the superior integrity achieved for ion-treated plasma polymer films is the predominant factor moderating the oxidation kinetics. This hypothesis is supported by taking the refractive index results (Fig. 4c) into account. These results indicated that highly cross-linked IPP structures are formed under the influence of energetic ion bombardment. A densely cross-linked structure provides lower mobility for structural elements including the secondary radicals, e.g. C–O–O·, generated as a result of oxidation (Fig. 5b). The limited segmental mobility reduces the chances of hydrogen abstraction by the secondary radicals formed during the oxidation process [67]. Such limited mobility leads to quick decay of these radicals because of their preferential recombination with each other described by the 'cage effect' [74]. Hence, adequate concentration of free radicals could not be regenerated within a highly cross-linked structure after long incubation times, eventually yielding the termination of the oxidation chain reactions.

Another possible explanation for the superior chemical stability of the IPP films compared to conventional plasma polymer films ($V_b = 0$) is the restricted access of O_2 and H_2O molecules to active radical sites. Oxidation and hydrolysis reactions may take place both on the surface and within the bulk of a polymeric material [75]. The latter, however, requires the intrusion of water molecules into the polymer network that is hampered by a highly cross-linked structure with great resistivity to permeation. Another possible reason for such great chemical stability is the termination of oxidation reactions due to the depletion of C–H groups over time and eventual unavailability of the abstractable hydrogen atoms. It has been previously reported that the termination of oxidation reactions in hydrocarbon-based plasma polymer films is linked with the lack of available C–H species [49,73]. This mechanism correlates well with our ERDA measurements (Fig. 2f) that confirmed a significantly lower hydrogen concentration for the PP film deposited at $V_b = -1000$ V compared to lower V_b values.

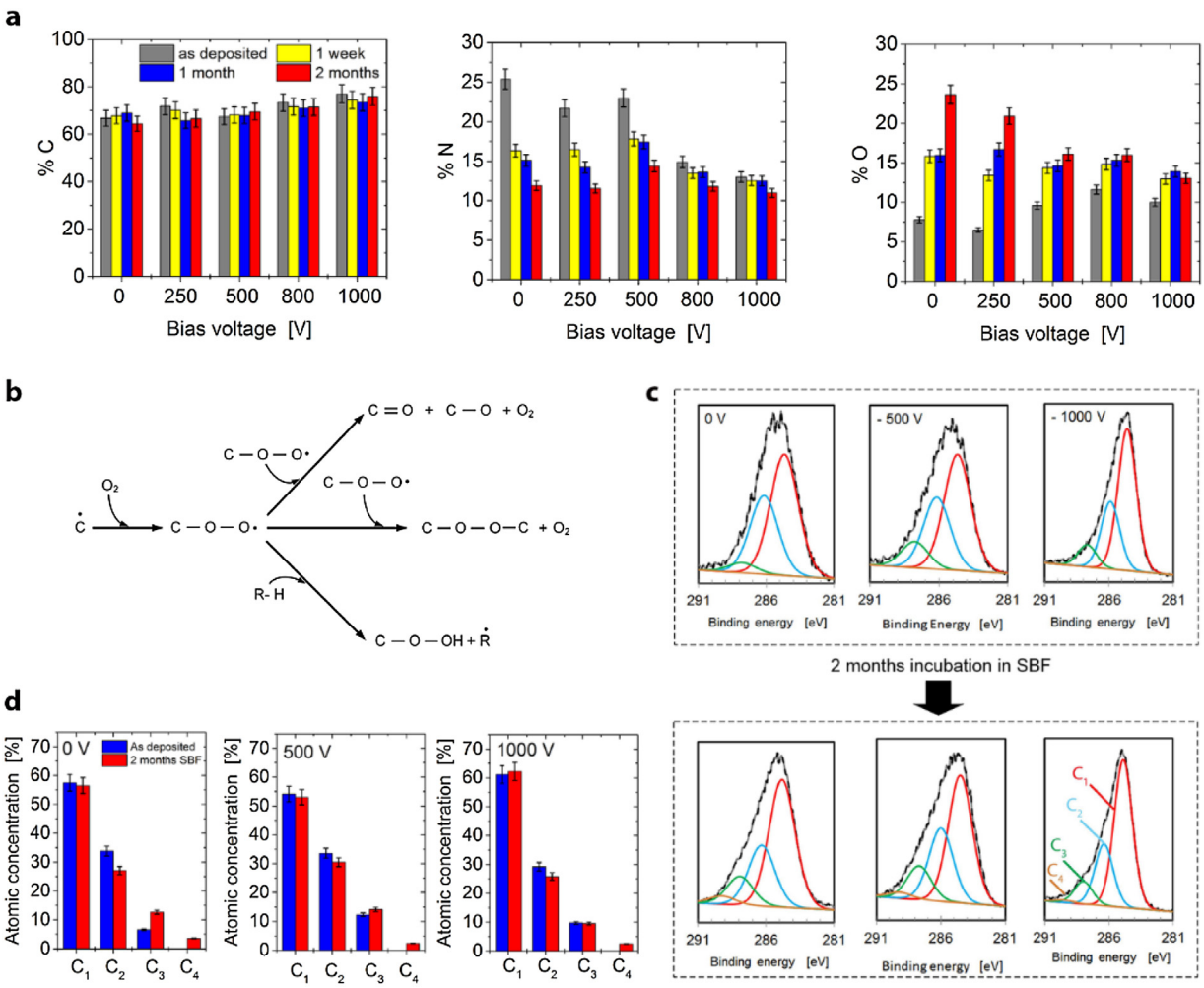

Fig. 5. Chemical stability of IPP films in simulated body fluid (SBF). (a) XPS elemental compositions of IPP films as a function of applied bias voltage before and after incubation in Tyrode's SBF solution for various durations. (b) Possible oxidation pathways initiated from a carbon-centered radical upon incubation of IPP films in SBF. (c) XPS C 1s high resolution spectra of IPP films before and after incubation in SBF for two months. The spectra were curve-fitted by four components: C_1: C–C/C–H, C_2: C–O/C–N, C_3: C=O/N–C=O, and C_4: COOH. (d) Atomic concentrations of peak-fitted C1s components of IPP films before and after incubation in SBF for two months.

3.2.2. *Physical stability*

We showed that the plasma polymer films treated with higher degrees of ion bombardment exhibit greater chemical stability in a simulated biological environment. However, the physical stability of a coating must also meet the demand for biological applications. An ideal, stable coating should resist any physical deformation in a form of thickness reduction, delamination, and swelling upon contact with biological media. To evaluate the physical stability of the films, we examined the changes in thicknesses, refractive index, and topology of the films after incubation in SBF.

The changes in thickness and refractive index values provide useful information on the extent of material loss from the film or swelling of the structure. The reduction of thickness is a measure of film solubility; whereas increases in the film thickness, accompanied by decreases in the refractive index, are indicative of the film swelling and penetration of water into the polymer network [19]. Fig. 6a shows thicknesses and refractive indices of IPP films as a function of applied bias voltage for various incubation times obtained by spectroscopic ellipsometry. For this analysis, the films were deposited on atomically smooth silicon wafers rather than titanium substrates to minimize the influence of roughness on the obtained data. The PP films deposited at bias voltages below −500 V were not stable in the SBF solution and were partially delaminated from the silicon surface even after only one-week incubation. However, no delamination was observed for these films deposited on titanium surfaces, as confirmed by the absence of titanium signals in the XPS spectra. We have recently shown that the greater interfacial adhesion of plasma polymer films deposited on titanium is due to the formation of strong metallic carbide/oxycarbide bonds at the interface during the initial stages of films growth [34]. Such behavior highlights the role of the substrate chemistry in determining physical stability of a plasma polymer film and suggests that early stages of plasma polymerization are strongly substrate-dependent. The IPP coating deposited at $V_b = -500$ V was stable for up to 1 month incubation in SBF but showed partial delamination after two months incubation. The IPP coatings deposited at $V_b > -500$ V showed minimal changes in the film thickness and refractive index after 1 week incubation, while a slight increase in thickness (by ~15%) accompanied by decreases in the refractive index (by ~2%) were observed after one month incubation. Further increasing the incubation duration to two months did not result in a noticeable change in the thickness and refractive index values. These changes are indicative of small degrees of film swelling upon incubation due to the removal of low-molecular weight, water-soluble species from the film structure as well as with penetration of water molecules into the polymer matrix and rearrangement of polymer chains [19,76].

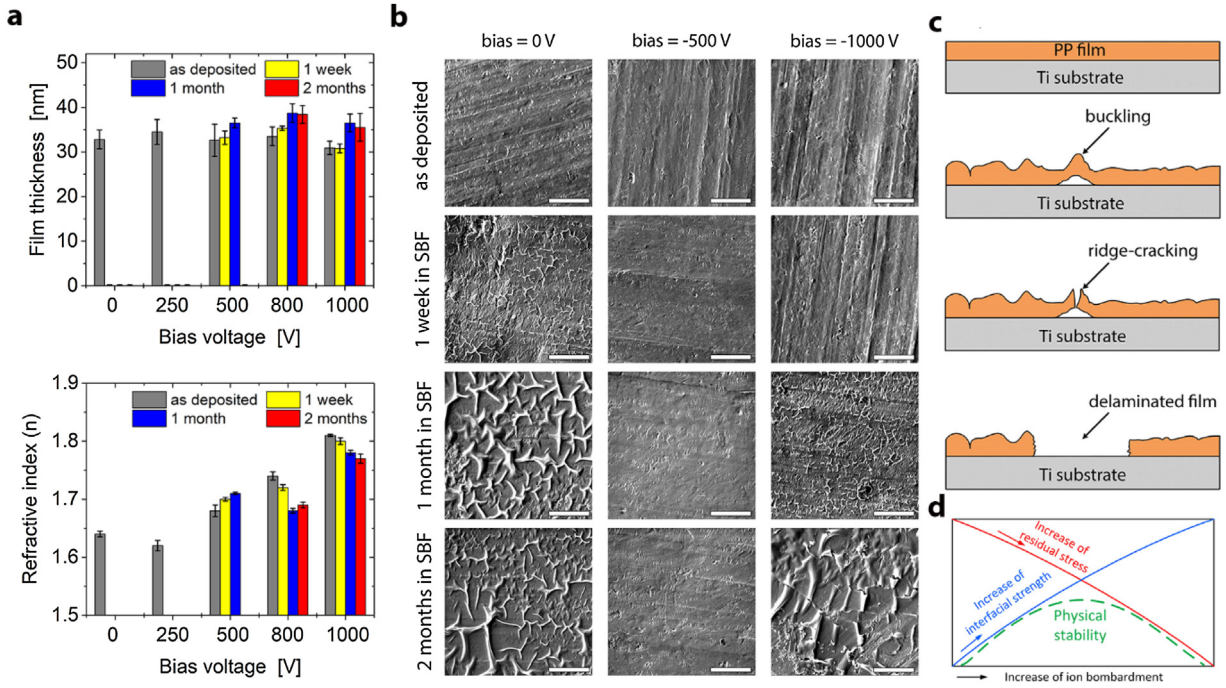

Fig. 6. Physical stability of IPP films in simulated body fluid (SBF). (a) Film thickness and refractive index (at λ = 630 nm) of IPP films as a function of applied bias voltage before and after incubation in Tyrode's SBF for various durations. (b) SEM images of IPP films deposited on titanium surfaces at bias voltages of 0, −500, and −1000 V before and after incubation in SBF. Scale bar = 10 μm (c) Schematic illustration of buckling formation in IPP films followed by the development of ridge cracks that results in the eventual delamination of the film from the titanium substrate. (d) Schematic illustration of changes in residual stress, interfacial strength, and physical stability of IPP films as a function of ion bombardment.

The degree of swelling in polymeric films depends on the average degree of cross-linking together with the topological distribution of cross-links [77]. As plasma polymer deposition of nanometre-thick films is expected to produce homogeneous structures [78], it is reasonable to only consider the cross-linking density as a major influencing factor in the swelling of the films. The excellent resistance to both swelling and film thickness reduction observed for the IPP films deposited at elevated ion bombardment conditions can be explained by their high degree of cross-linking density as suggested by their relatively large refractive index values (Fig. 4c).

The topographical examination of IPP films upon incubation in Tyrode's SBF provides further insight into their physical robustness. SEM images of IPP-coated titanium surfaces before and after incubation in SBF are shown in Fig. 6b. The IPP coatings before incubation are smooth and follow the topography of the underlying titanium surface. The formation of buckling features is observed for the films prepared at $V_b = 0$ and −1000 V for incubation times longer than 1 week and 1 month, respectively. In contrast, no evidence of buckling, cracking, or delamination is witnessed for the film prepared at $V_b = -500$ V even after two months incubation in SBF.

It is energetically favorable for a residually compressed film to buckle out of the substrate plane once the compressive force exceeds a critical value [79]. Hence, polymeric films with large degrees of compressive residual stress and/or low adhesion to the substrate are highly susceptible to form buckles. The great physical stability exhibited by the film deposited at $V_b = -500$ V is well explained with the XPS results that suggested the formation of metallic carbide bonds at the film-substrate interface. We, therefore, suggest that such a chemical linkage formed at early stages of deposition 'pins' the film to the substrate, preventing the film from swelling and delamination; a hypothesis also supported by the nano-scratch results (Fig. 4f). The formation of buckling features observed for the coating deposited at $V_b = -1000$ V, however, correlates well with its large compressive residual stress measured from the radius of curvature (Fig. 4e) and also with its cohesive failure in the nano-scratch test (Fig. 4f). The highly cross-linked structure of this film constrains the rearrangement of polymer chains, making the film less accommodating to residual stresses [76] that are relieved ultimately by buckling formation. Few cracks at low micrometer-length scale are formed on the buckles of this film after two months incubation. The formation of such ridge-cracks can be linked to the tensile strength induced by the formation of buckles and the relatively high stiffness of the film, i.e. large modulus of elasticity, as suggested by nano-indentation data (Fig. 4d). The buckling formation followed by the development of ridge cracks leads to the eventual delamination of the film from the titanium substrate as illustrated schematically in Fig. 6c. According to the physical stability results, it can be concluded that the excellent robustness of the IPP film deposited under moderate ion bombardment conditions ($V_b = -500$ V) is correlated with an optimum balance achieved between the film-substrate adhesion and the degree of residual stress, as depicted in Fig. 6d. These results underpin a critical advantage of ion-assisted plasma polymerization compared to the conventional plasma polymerization. Even if the conventional plasma polymer film (control sample, $V_b = 0$) could show equivalent, reagent-free capability to immobilize protein molecules, its performance in practical applications will be limited by failure upon abrasion, associated with surgical insertion, and/or immersion in corrosive body fluids.

3.3. Biomolecular-functionalization and analyses of biological responses

3.3.1. Protein covalent functionalization

We used fibronectin (FN) and bone morphogenetic protein 2 (BMP-2) as model proteins to evaluate the ability of the optimized IPP film to covalently attach a layer of biomolecules. Fibronectin is a glycoprotein found in blood plasma and in the extracellular matrix

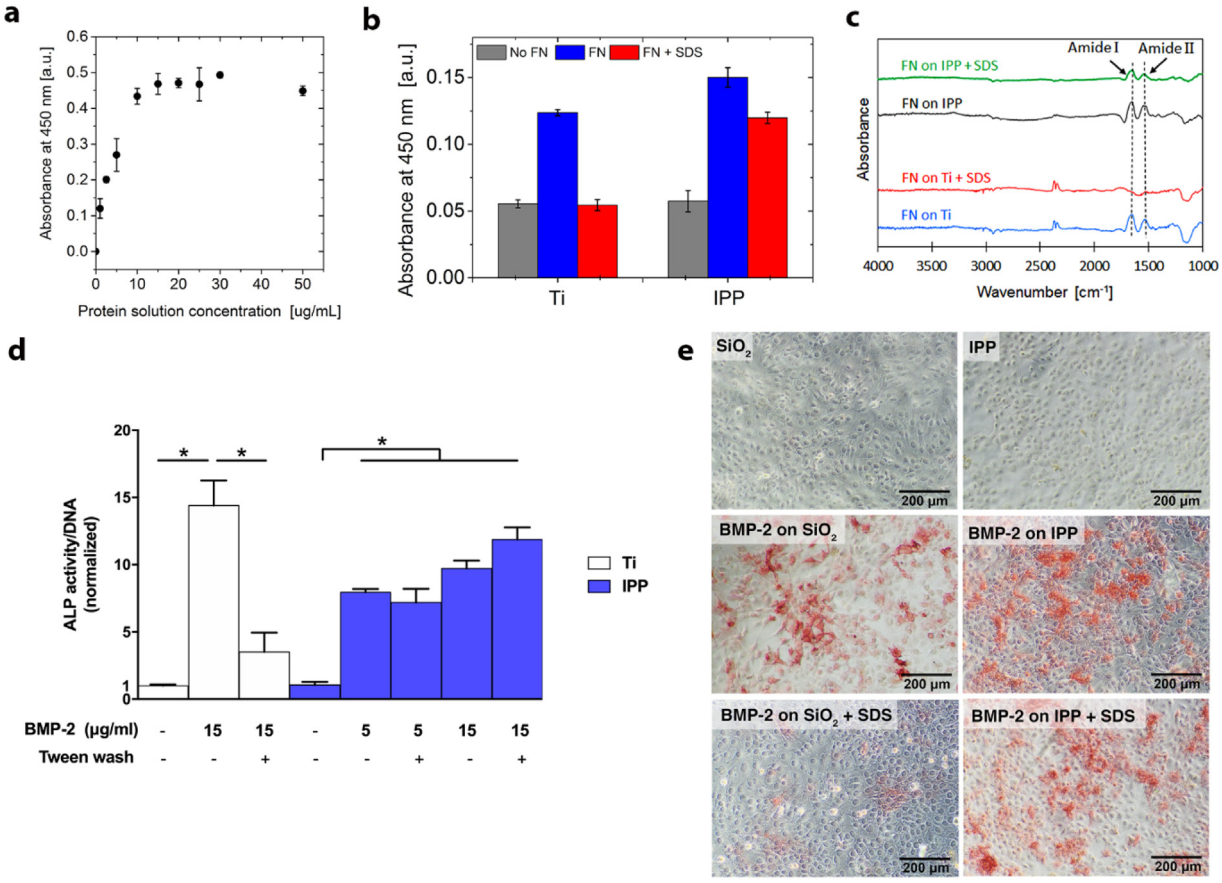

Fig. 7. Protein covalent functionalization of Ti through IPP interlayer. (a) ELISA detection of surface-bound fibronectin as a function of protein concentration in the immobilization solution. (b) ELISA detection of surface-bound protein for uncoated and IPP film-coated Ti surfaces incubated in fibronectin solution before and after SDS washing. (c) ATR FT-IR spectra of fibronectin bound to bare and IPP-coated Ti with and without SDS washing. The spectra of IPP-coated titanium before fibronectin attachment is subtracted from the presented spectra. (d) Day 3 ALP activity per DNA content was quantified in ATDC5 cells to show BMP-2 bioactivity on non-coated and IPP-coated Ti foils with or without Tween-20 washing. ALP activity/DNA was normalized to the value obtained for the untreated Ti. Data represent the mean ± SD (n = 3 samples). *$p < 0.05$. (e) Day 3 ALP staining (red) was performed on ATDC5 cells to show BMP-2 bioactivity on non-coated and IPP-coated glass coverslips (SiO_2) with or without SDS washing. Surfaces were functionalized with 15 μg/ml BMP-2.

that mediates a variety of biological processes including regulation of thrombus formation and cellular adhesion, migration, growth, and differentiation [80,81]. Fibronectin contains the canonical Arg-Gly-Asp (RGD) sequence motif, facilitating interactions with a vast number of cell surface integrins, and subsequently influencing cell behavior. In the context of osteoblasts, fibronectin is a critical mediator of attachment, differentiation [82], and survival [83], through a select group of integrins, including α5β1 [84].

A titration of fibronectin was initially coated on the samples to find the optimum concentration of protein in solution providing maximum surface activity. Fig. 7a shows ELISA detection of surface-bound fibronectin as a function of protein concentration in the immobilization solution. The optimum fibronectin solution concentration is approximately 15 μg/ml; as the ELISA signal plateaus for higher concentrations. This optimum concentration is significantly lower than that reported for other surfaces. Heller et al. immobilized fibronectin on an allylamine plasma polymer-coated gold surface using α, ω-bis-N-hydroxysuccinimide polyethylene glycol (Di-NHS linker) at 1000 μg/mL [85]. The same concentration was utilized for chemical immobilization on polydopamine [86]. Attachment through tresylation, a chemisorption process, required a 100 μg/mL fibronectin solution [87,88]. The immobilization of fibronectin through radicals embedded within the IPP coating results in a more effective loading of protein with the optimal concentration approximately a tenth of that required for other immobilization approaches. We used the optimum fibronectin concentration of 15 μg/ml for the covalent attachment and osteoblast cellular interaction experiments.

Covalent attachment to the optimized coating was evaluated by incubating the IPP-coated titanium in the fibronectin buffer solution followed by sodium dodecyl sulfate (SDS) washing. SDS is a strong detergent that removes proteins physisorbed on surfaces, while leaving covalently bonded molecules intact [89,90]. XPS measurements of the protein molecules immobilized on IPP films did not provide conclusive results, as the protein molecules could not be distinguished reliably from the underlying polymer film due to their similar elemental compositions. We, therefore, used ELISA and ATR-FTIR analysis to detect the surface-attached protein molecules.

The ELISA results for uncoated and IPP-coated Ti surfaces incubated in fibronectin solution before and after SDS washing are plotted in Fig. 7b. After the vigorous SDS washing, approximately 80% of immobilized fibronectin was still present on the IPP surface, whereas the absorbance values for the bare Ti were reduced almost to the background level, indicating that only a small fraction of the protein (~15%) remained on the surface. The ELISA results are confirmed by ATR FT-IR spectra of fibronectin bound to uncoated and IPP-coated Ti with and without SDS washing (Fig. 7c). The spectra of uncoated titanium or IPP-coated titanium (without fibronectin) were subtracted from the spectra of samples incubated in fibronectin solution to reveal the peaks associated with the protein molecules. The peaks observed at 1650 and 1540 cm^{-1} are assigned to Amide I and Amide II vibrational modes of amide

bonds in the backbones of the protein molecules, respectively. For the uncoated Ti incubated in fibronectin solution, the amide peaks are observed only in the absence of SDS washing; whereas on the IPP-coated Ti, these peaks are present both before and after SDS washing.

To test the hypothesis that IPP coatings can be used to anchor clinically-applied molecules for enhanced osteogenesis, we investigated the covalent binding of bone-morphogenetic protein (BMP)-2 to the IPP-coated surfaces. BMP-2 is one of the few alternatives for autologous bone transplantation in the treatment of critical size bone defects [91], but the current delivery system using a collagen sponge is associated with off-target effects and suboptimal efficiency [92,93]. Hence, the covalent binding of BMP-2 onto implant surfaces, may result in localized, prolonged activity, and improved outcomes [94]. Using the ATDC5 cell line as reporter cells for BMP-2 [38], we found that BMP-2 remained bioactive after conjugation to IPP coated surfaces (Fig. 7d, e). The IPP surface was negatively charged at neutral pH with a zeta potential of approximately −15 mV as measured by an electrokinetic analyzer. The water and diiodomethane contact angles of the IPP coating, measured within 30 min after the deposition, were $(47.3 \pm 0.8)^\circ$ and $(17.8 \pm 0.2)^\circ$, respectively; giving a total surface free energy of 65.9 ± 0.1 mJ m^{-2}. This mildly hydrophilic character of the surface allows for BMP-2 molecules to retain their native conformation and therefore their bioactivity [95].

Furthermore, bioactivity of IPP-BMP-2 surfaces remained unchanged upon washing with Tween-20 detergent as opposed to physisorbed BMP-2 on uncoated Ti (Fig. 7d). The significant reduction of activity observed for Ti-BMP-2 surfaces is most likely due the removal of BMP-2 molecules physically attached to the surfaces in the absence of the IPP coating. These results are further endorsed with data obtained after an even more severe washing protocol using SDS (Fig. 7e) that confirms the covalent immobilization of BMP-2 molecules on the IPP-coated Ti. Together, these data attest the excellent covalent binding capacity of the IPP coating and the weakly bound nature of the protein physisorbed on the bare Ti substrates. It can be, therefore, concluded that IPP coatings allow strong, elution-resistant binding of various biomolecules without hampering their bioactivity.

3.3.2. Primary osteoblast cellular interactions

The biofunctionality of a bone-implant interface strongly depends on both bone-inductive and bone-conductive mechanisms provided by bone-residing cells [96]. Therefore, we quantified primary osteoblast (OB) attachment, spreading, and proliferation on as-deposited IPP films followed by immobilization of fibronectin. Mouse primary osteoblast adhesion to the IPP film was similar to titanium controls, but significantly increased for fibronectin coated-IPP (Fig. 8a). The IPP film alone caused a non-significant $17 \pm 4\%$ (p = ns) increase in the number of attached cells, while coating IPP with fibronectin increased the number of attached cells by $39 \pm 5\%$ ($p < 0.01$) and spreading of osteoblasts by $73 \pm 3\%$ ($p < 0.001$) compared to bare titanium (Fig. 8b). Representative images showing staining of actin fibers clearly demonstrate the significantly enhanced spreading on IPP + FN (Fig. 8c). Proliferation of OBs over longer time points also demonstrated a benefit for IPP + FN (Fig. 8d). At day 3, all conditions were equivalent, while at day 6 and 10 marginal improvements in proliferation on IPP + FN did not reach significance. However, by day 14, IPP + FN was found to be $40 \pm 6\%$ greater than titanium only ($p < 0.001$) and $20 \pm 6\%$ higher than IPP alone ($p < 0.05$). Cells utilize integrins for the attachment to specific cell binding sites displayed by ECM proteins such as fibronectin. These integrins link the cell cytoskeleton to the IPP surface through the immobilized fibronectin molecules [97]. The improvements in the interactions of osteoblast cells on the FB-coated surface is due to this well-known function of fibronectin.

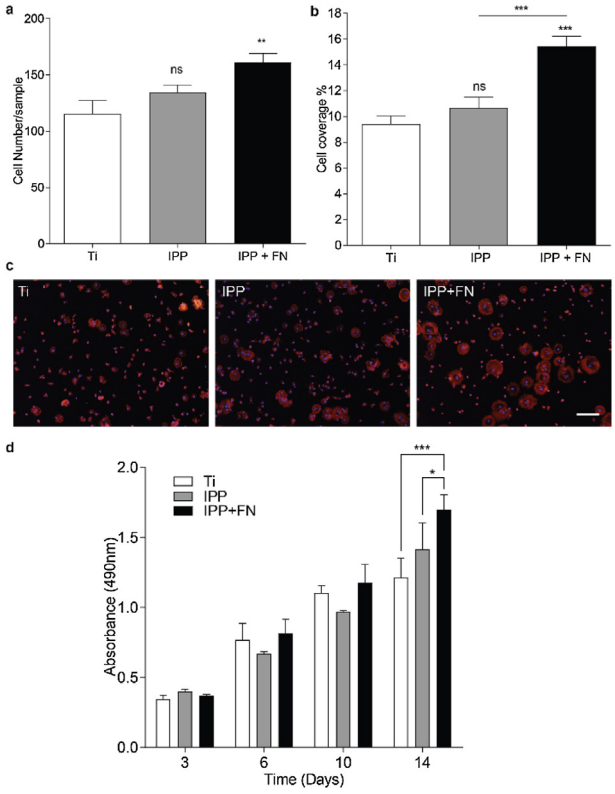

Fig. 8. Primary osteoblast cellular interactions. Primary mouse osteoblast (a) attachment to, (b) and spreading on Ti, IPP and IPP + fibronectin (FN) surfaces (c) Representative images of osteoblast spreading demonstrating changes to the actin stained cytoskeletons of the cells (red). Cell nuclei are stained blue. (d) Osteoblast proliferation on the same surfaces at 3, 6, 10 and 14 day time points. Scale bar = 100 μm.

The fibronectin-mediated attachment and proliferation of osteoblasts has been widely reported before for physically adsorbed fibronectin on Ti surfaces [97–99]. However, as explained in the Introduction section, physical adsorption is not a suitable biofunctionalization approach, as physisorbed proteins suffer from displacement and denaturation in the biological medium due to processes such as the Vroman effect [10].

3.3.3. Viability and osteogenesis of human MSCs

The healing of large bone defects relies on the recruitment of undifferentiated MSCs from the bone marrow and their differentiation toward the osteogenic lineage [96,100]. This property of MSCs is thought to underlie the osteoinductive effect of the clinically-used growth factor BMP-2. [101] Therefore, MSCs were used as the cell source to study the effects of BMP-2 immobilization on Ti and IPP films. First, it was found that the IPP films support normal MSC adhesion and expansion. In fact, the number of surface-attached MSCs on the IPP coating was always greater than that found on bare Ti as shown by the higher metabolic activity up to five days of culture (Fig. 9a). This suggests that the IPP film alone favors the adhesion and/or proliferation of MSCs, even in the absence of biomolecules promoting cell binding such as fibronectin. In line, qualitative staining for live and dead cells demonstrated no cytotoxic activity of the IPP surfaces on MSCs and confirmed their adhesion and spreading on IPP and bare Ti surfaces (Fig. 9b).

To elucidate whether IPP + BMP-2 functionalization would lead to superior osteoblast differentiation over physisorbed BMP-2 coatings, we measured osteocalcin expression. Osteocalcin was selected as a marker of MSC osteogenic differentiation, because it is a bone-specific protein synthesized by osteoblasts [41].

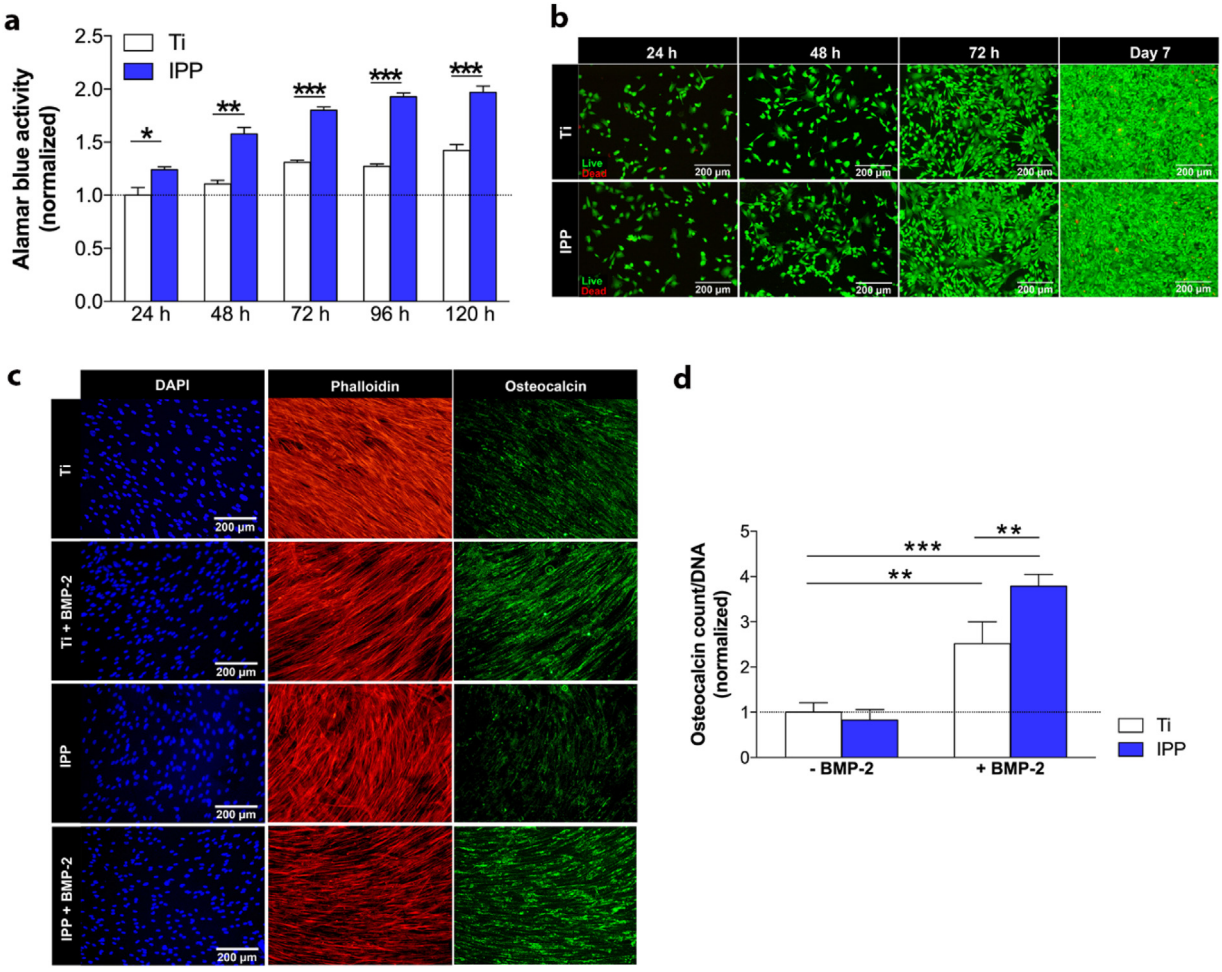

Fig. 9. Viability and osteogenesis of MSCs cultured after surface functionalization. (A) Metabolic activity of human MSCs cultured on untreated or IPP-treated Ti foils as measured by the Alamar Blue assay. Metabolic activity was normalized to the value obtained for untreated Ti at 24 h. (B) Live (green)/dead (red) staining performed on MSCs cultured on untreated and IPP-treated Ti foils to demonstrate cell attachment and proliferation over time. (C) Day 14 immunocytochemical staining for osteocalcin (green) was performed to show osteoblast differentiation on Ti or IPP surfaces, with and without BMP-2 functionalization. Cells were counterstained with DAPI (blue, cell nuclei) and phalloidin (orange, cytoskeleton). (D) Day 14 osteocalcin expression was quantified by counting the osteocalcin-positive pixels and normalizing for the DNA content measured in each group. Data represent the mean ± SD (n = 3 samples). *p < 0.05, ** p < 0.005, ***p < 0.0005.

Moreover, as a late osteogenic marker, enhanced osteocalcin expression will be more likely realized by sustained BMP-2 signaling following the covalent binding. While both physically adsorbed and IPP-immobilized BMP-2 seemingly enhanced the day 14 osteocalcin expression in MSCs (Fig. 9c), the IPP + BMP-2 surfaces induced the highest quantitative levels of osteocalcin expression per cell number (Fig. 9d).

These data collectively show that IPP coatings are biocompatible for human MSCs, and that IPP + BMP-2 coatings elicit the highest level of osteoblast differentiation. These results also imply that the covalent binding of BMP-2 molecules to Ti prolonged their bioactivity as compared to those simply physisorbed on bare Ti. The lower bioactivity of physisorbed BMP-2 is most likely due to competitive protein adsorption-desorption taking place with the presence of other biomolecules in the serum component of the medium, but more elaborated studies are required for conclusive proof. If this is the case, then the advantage provided by IPP, that facilitated covalent tethering of biosignalling molecules such as BMP-2, is likely understated in our experiments. Despite the medium refreshments performed every fourth day, the confined wells used for in vitro assessments would maintain the local BMP-2 concentration at artificially higher levels post protein desorption compared to that in vivo where desorbed proteins are free to diffuse throughout the body. Additional follow-up research is also required to elucidate whether IPP surfaces can also be used to improve osteoinduction for biodegradable bone substitute materials. Of these, calcium phosphates-based products are interesting target materials; since they are already widely available [102], but still require functionalization with bone-stimulating factors to match the properties of autologous bone [103,104].

We believe that our findings on the development of functional and strongly robust IPP coatings have great implications for the fabrication of bio-interfaces that need to survive abrasive effects of surgical insertion and long-term immersion in corrosive body fluids. The application of these coatings holds great promise particularly for the surface modification of bone implants where requirements for interfacial robustness are very demanding.

4. Conclusions

In the pursuit of a simple platform technology for the fabrication of bio-functionalized coatings, we showed that energetic ion bombardment of a growing plasma polymer film through pulse biasing of the substrate is beneficial for two reasons. First, it results in high concentrations of radicals that serve as reactive sites for the covalent attachment of biomolecules. Second, it yields an increase in the degree of cross-linking in the polymer structure and also a tough

interface with the substrate when applied to a carbide-forming material. These findings have important implications for the surface engineering of implantable devices as coatings with the combination of such properties cannot be produced, in a single-step, using conventional plasma polymerization processes. The ion-assisted plasma polymerized (IPP) films were resistant to abrasive damage and showed exceptional physico-chemical stability as necessary for orthopedic applications. When placed under physiological conditions for two months, the optimized films exhibited great chemical stability due to their highly cross-linked structure, restricting the intrusion of water molecules into the polymer network and moderating the oxidation kinetics. In vitro studies were carried out to exemplify one potential application to bone implantable devices. IPP films functionalized with fibronectin enhanced the attachment, spreading, and proliferation of primary mouse osteoblasts; suggesting the bioactive presentation of fibronectin. For MSCs, IPP films alone promoted cell adhesion and proliferation even in the absence of surface-attached proteins. Furthermore, IPP films covalently functionalized with BMP-2 led to enhanced osteoblast differentiation in MSCs as compared to physisorbed BMP-2 on bare Ti. Our findings indicate that the technology presented here is a leap forward in the fabrication of robust bio-functional interfaces that can be readily applied to a wide range of implants, and in particular in connection with bone integration.

Data availability

The authors declare that all data supporting the findings of this study are available within the article and its supplementary information files or from the corresponding author upon request.

Acknowledgments

This research was financially supported by Australian Research Council (ARC) and the University of Sydney–Utrecht University Partnership Collaboration Award. The authors acknowledge the facilities, scientific and technical assistance of Microscopy Australia at the University of South Australia, a facility that is funded by the University of South Australia, the State and Federal Governments. We are thankful to Dr Lewis Martin for preparing the schematic illustration shown in Fig. 1a and b.

Appendix A. Supplementary data

Supplementary data associated with this article can be found, in the online version, at doi:10.1016/j.apmt.2019.07.002.

References

[1] W. Chrzanowski, J.H. Lee, A. Kondyurin, M.S. Lord, J.-H. Jang, H.-W. Kim, M.M.M. Bilek, Nano-bio-chemical braille for cells: the regulation of stem cell responses using bi-functional surfaces, Adv. Funct. Mater. 25 (2) (2015) 193–205.
[2] S. Torgbo, P. Sukyai, Bacterial cellulose-based scaffold materials for bone tissue engineering, Appl. Mater. Today 11 (2018) 34–49.
[3] M. Croes, S. Bakhshandeh, I.A.J. van Hengel, K. Lietaert, K.P.M. van Kessel, B. Pouran, B.C.H. van der Wal, H.C. Vogely, W. Van Hecke, A.C. Fluit, C.H.E. Boel, J. Alblas, A.A. Zadpoor, H. Weinans, S. Amin Yavari, Antibacterial and immunogenic behavior of silver coatings on additively manufactured porous titanium, Acta Biomater. 81 (2018) 315–327.
[4] L. Liu, Y. He, X. Shi, H. Gao, Y. Wang, Z. Lin, Phosphocreatine-modified chitosan porous scaffolds promote mineralization and osteogenesis in vitro and in vivo, Appl. Mater. Today 12 (2018) 21–33.
[5] X. Zhang, J. Nie, X. Yang, Z. Liu, W. Guo, J. Qiu, S. Wang, X. Yu, Y. Guan, H. Liu, Nanostructured molybdenum disulfide biointerface for adhesion and osteogenic differentiation of mesenchymal stem cells, Appl. Mater. Today 10 (2018) 164–172.
[6] C.A. Murphy, J.B. Costa, J. Silva-Correia, J.M. Oliveira, R.L. Reis, M.N. Collins, Biopolymers and polymers in the search of alternative treatments for meniscal regeneration: state of the art and future trends, Appl. Mater. Today 12 (2018) 51–71.
[7] R. Ganesan, B. Akhavan, M.A. Hiob, D.R. McKenzie, A.S. Weiss, M.M.M. Bilek, HiPIMS carbon coatings show covalent protein binding that imparts enhanced hemocompatibility, Carbon 139 (2018) 118–128.
[8] S. Kumar, S. Raj, K. Sarkar, K. Chatterjee, Engineering a multi-biofunctional composite using poly (ethylenimine) decorated graphene oxide for bone tissue regeneration, Nanoscale 8 (12) (2016) 6820–6836.
[9] S.A. Yavari, J. van der Stok, Y.C. Chai, R. Wauthle, Z.T. Birgani, P. Habibovic, M. Mulier, J. Schrooten, H. Weinans, A.A. Zadpoor, Bone regeneration performance of surface-treated porous titanium, Biomaterials 35 (24) (2014) 6172–6181.
[10] L. Vroman, Effect of adsorbed proteins on the wettability of hydrophilic and hydrophobic solids, Nature 196 (4853) (1962) 476.
[11] H.-Y. Ao, Y.-T. Xie, S.-B. Yang, X.-D. Wu, K. Li, X.-B. Zheng, T.-T. Tang, Covalently immobilised type I collagen facilitates osteoconduction and osseointegration of titanium coated implants, J. Orthop. Transl. 5 (2016) 16–25.
[12] S.E. Kim, C.-S. Kim, Y.-P. Yun, D.H. Yang, K. Park, S.E. Kim, C.-M. Jeong, J.-B. Huh, Improving osteoblast functions and bone formation upon BMP-2 immobilization on titanium modified with heparin, Carbohydr. Polym. 114 (2014) 123–132.
[13] A. Michelmore, D.A. Steele, J.D. Whittle, J.W. Bradley, R.D. Short, Nanoscale deposition of chemically functionalised films via plasma polymerisation, RSC Adv. 3 (33) (2013) 13540–13557.
[14] A. Nikiforov, X.L. Deng, Q. Xiong, U. Cvelbar, N. De Geyter, R. Morent, C. Leys, Non-thermal plasma technology for the development of antimicrobial surfaces: a review, J. Phys. D: Appl. Phys. 49 (20) (2016) 8.
[15] L.E. Smith, C. Bryant, M. Krasowska, A.J. Cowin, J.D. Whittle, S. MacNeil, R.D. Short, Haptotatic plasma polymerized surfaces for rapid tissue regeneration and wound healing, ACS Appl. Mater. Interfaces 8 (48) (2016) 32675–32687.
[16] B.R. Coad, M. Jasieniak, S.S. Griesser, H.J. Griesser, Controlled covalent surface immobilisation of proteins and peptides using plasma methods, Surf. Coat. Technol. 233 (2013) 169–177.
[17] W. Ogieglo, H. Wormeester, K.J. Eichhorn, M. Wessling, N.E. Benes, In situ ellipsometry studies on swelling of thin polymer films: a review, Prog. Polym. Sci. 42 (2015) 42–78.
[18] F. Truica-Marasescu, M.R. Wertheimer, Nitrogen-rich plasma-polymer films for biomedical applications, Plasma Process. Polym. 5 (1) (2008) 44–57.
[19] L.Q. Chu, Q. Zhang, R. Forch, Surface plasmon-based techniques for the analysis of plasma deposited functional films and surfaces, Plasma Process. Polym. 12 (9) (2015) 941–952.
[20] A. Manakhov, L. Zajickova, M. Elias, J. Cechal, J. Polcak, J. Hnilica, S. Bittnerova, D. Necas, Optimization of cyclopropylamine plasma polymerization toward enhanced layer stability in contact with water, Plasma Process. Polym. 11 (6) (2014) 532–544.
[21] M. Laurent, J. Koehler, G. Sabbatier, C.A. Hoesli, N. Gherardi, G. Laroche, Atmospheric pressure plasma polymer of ethyl lactate: in vitro degradation and cell viability studies, Plasma Process. Polym. 13 (7) (2016) 711–721.
[22] L. Detomaso, R. Gristina, G.S. Senesi, R. d'Agostino, P. Favia, Stable plasma-deposited acrylic acid surfaces for cell culture applications, Biomaterials 26 (18) (2005) 3831–3841.
[23] B. Akhavan, K. Jarvis, P. Majewski, Plasma polymerization of sulfur-rich and water-stable coatings on silica particles, Surf. Coat. Technol. 264 (2015) 72–79.
[24] Q. Chen, Stability of an ultrathin plasma polymerized film in aqueous solution: in situ detection by surface plasmon resonance, J. Phys. Chem. B 110 (18) (2006) 9231–9235.
[25] J.C. Ruiz, A. St-Georges-Robillard, C. Theresy, S. Lerouge, M.R. Wertheimer, Fabrication and characterisation of amine-rich organic thin films: focus on stability, Plasma Process. Polym. 7 (9–10) (2010) 737–753.
[26] L.J. Martin, B. Akhavan, M.M. Bilek, Electric fields control the orientation of peptides irreversibly immobilized on radical-functionalized surfaces, Nat. Commun. 9 (1) (2018) 357.
[27] B. Akhavan, T.D. Michl, C. Giles, K. Ho, L. Martin, O. Sharifahmadian, S.G. Wise, B.R. Coad, N. Kumar, H.J. Griesser, Plasma activated coatings with dual action against fungi and bacteria, Appl. Mater. Today 12 (2018) 72–84.
[28] M. Santos, E.C. Filipe, P.L. Michael, J.C. Hung, S.G. Wise, M.M.M. Bilek, Mechanically robust plasma-activated interfaces optimized for vascular stent applications, ACS Appl. Mater. Interfaces 8 (15) (2016) 9635–9650.
[29] C.A. Stewart, B. Akhavan, J. Hung, S. Bao, J.-H. Jang, S.G. Wise, M.M. Bilek, Multifunctional protein-immobilized plasma polymer films for orthopedic applications, ACS Biomater. Sci. Eng. 4 (12) (2018) 4084–4094.
[30] B. Akhavan, S. Bakhshandeh, H. Najafi-Ashtiani, A.C. Fluit, E. Boel, C. Vogely, B.C.H. van der Wal, A.A. Zadpoor, H. Weinans, W.E. Hennink, M.M. Bilek, S. Amin Yavari, Direct covalent attachment of silver nanoparticles on radical-rich plasma polymer films for antibacterial applications, J. Mater. Chem. B (2018).
[31] C.A. Stewart, B. Akhavan, M. Santos, J. Hung, C.L. Hawkins, B. Bao, S.G. Wise, M.M. Bilek, Cellular responses to radical propagation from ion-implanted plasma polymer surfaces, Appl. Surf. Sci. 456 (2018) 701–710.
[32] M.M.M. Bilek, D.V. Bax, A. Kondyurin, Y.B. Yin, N.J. Nosworthy, K. Fisher, A. Waterhouse, A.S. Weiss, C.G. dos Remedios, D.R. McKenzie, Free radical functionalization of surfaces to prevent adverse responses to biomedical devices, Proc. Natl. Acad. Sci. U. S. A. 108 (35) (2011) 14405–14410.

[33] B. Akhavan, M. Bilek, Controlled deposition of plasma activated coatings on zirconium substrates, in: B.J. Eggleton, S. Palomba (Eds.), Micro + Nano Materials, Devices, and Systems, SPIE-Int Soc Optical Engineering, Bellingham, 2015.
[34] B. Akhavan, S.G. Wise, M.M.M. Bilek, Substrate-regulated growth of plasma-polymerized films on carbide-forming metals, Langmuir 32 (42) (2016) 10835–10843.
[35] W.C. Oliver, G.M. Pharr, Measurement of hardness and elastic modulus by instrumented indentation: advances in understanding and refinements to methodology, J. Mater. Res. 19 (1) (2004) 3–20.
[36] C. Zhai, Y. Gan, D. Hanaor, G. Proust, D. Retraint, The role of surface structure in normal contact stiffness, Exp. Mech. 56 (3) (2016) 359–368.
[37] A.D. Bakker, J. Klein-Nulend, Osteoblast isolation from murine calvaria and long bones, in: Bone Research Protocols, Springer, 2012, pp. 19–29.
[38] L. Loozen, A. Vandersteen, A. Kragten, F. Öner, W. Dhert, M. Kruyt, J. Alblas, Bone formation by heterodimers through non-viral gene delivery of BMP-2/6 and BMP-2/7, Eur. Cells Mater. 35 (2018) 195–208.
[39] M. Croes, F.C. Öner, D. van Neerven, E. Sabir, M.C. Kruyt, T.J. Blokhuis, W.J. Dhert, J. Alblas, Proinflammatory T cells and IL-17 stimulate osteoblast differentiation, Bone 84 (2016) 262–270.
[40] M. Dominici, K. Le Blanc, I. Mueller, I. Slaper-Cortenbach, F.C. Marini, D.S. Krause, R.J. Deans, A. Keating, D.J. Prockop, E.M. Horwitz, Minimal criteria for defining multipotent mesenchymal stromal cells. The International Society for Cellular Therapy position statement, Cytotherapy 8 (4) (2006) 315–317.
[41] P. Ducy, G. Karsenty, Two distinct osteoblast-specific cis-acting elements control expression of a mouse osteocalcin gene, Mol. Cell. Biol. 15 (4) (1995) 1858–1869.
[42] D. Hegemann, B. Hanselmann, N. Blanchard, M. Amberg, Plasma-substrate interaction during plasma deposition on polymers, Contrib. Plasma Phys. 54 (2) (2014) 162–169.
[43] T.D. Michl, B.R. Coad, M. Doran, A. Husler, J.D.P. Valentin, K. Vasilev, H.J. Griesser, Plasma polymerization of 1,1,1-trichloroethane yields a coating with robust antibacterial surface properties, RSC Adv. 4 (52) (2014) 27604–27606.
[44] B. Akhavan, K. Jarvis, P. Majewski, Development of negatively charged particulate surfaces through a dry plasma-assisted approach, RSC Adv. 5 (17) (2015) 12910–12921.
[45] N.A. Bullett, J.D. Whittle, R.D. Short, C.W.I. Douglas, Adsorption of immunoglobulin G to plasma-co-polymer surfaces of acrylic acid and 1,7-octadiene, J. Mater. Chem. 13 (7) (2003) 1546–1553.
[46] B. Akhavan, K. Jarvis, P. Majewski, Evolution of hydrophobicity in plasma polymerised 1,7-octadiene films, Plasma Process. Polym. 10 (11) (2013) 1018–1029.
[47] M. Lejeune, M. Berlahsen, P. Lemoine, Effect of air post contamination on mechanical properties of amorphous carbon nitride thin films, Solid State Commun. 135 (7) (2005) 434–439.
[48] D. Zeniieh, A.M. Rostas, E. Schleicher, L. Ledernez, S. Weber, G. Urban, The effect of low pressure plasma polymerization modes on the properties of the deposited plasma polymers, Plasma Process. Polym. 13 (7) (2016) 744–751.
[49] T.R. Gengenbach, Z.R. Vasic, R.C. Chatelier, H.J. Griesser, A multi-technique study of the spontaneous oxidation of n-hexane plasma polymers, J. Polym. Sci. A: Polym. Chem. 32 (8) (1994) 1399–1414.
[50] N. Stojilovic, Why can't we see hydrogen in X-ray photoelectron spectroscopy? J. Chem. Educ. 89 (10) (2012) 1331–1332.
[51] J. Zou, K. Reichelt, K. Schmidt, B. Dischler, The deposition and study of hard carbon films, J. Appl. Phys. 65 (10) (1989) 3914–3918.
[52] C.F.A. Alves, F. Oliveira, I. Carvalho, A.P. Piedade, S. Carvalho, Influence of albumin on the tribological behavior of Ag-Ti (C, N) thin films for orthopedic implants, Mater. Sci. Eng. C: Mater. Biol. Appl. 34 (2014) 22–28.
[53] X.H. Xia, Y.Q. Zhang, D.L. Chao, Q.Q. Xiong, Z.X. Fan, X.L. Tong, J.P. Tu, H. Zhang, H.J. Fan, Tubular TiC fibre nanostructures as supercapacitor electrode materials with stable cycling life and wide-temperature performance, Energy Environ. Sci. 8 (5) (2015) 1559–1568.
[54] J. Pouilleau, D. Devilliers, H. Groult, P. Marcus, Surface study of a titanium-based ceramic electrode material by X-ray photoelectron spectroscopy, J. Mater. Sci. 32 (21) (1997) 5645–5651.
[55] M.W. Chase, JANAF Thermochemical Tables, fourth edition, American Institute of Physics for the National Bureau of Standards, American Chemical Society, New York, 1986.
[56] D. Hegemann, E. Körner, K. Albrecht, U. Schütz, S. Guimond, Growth mechanism of oxygen-containing functional plasma polymers, Plasma Process. Polym. 7 (11) (2010) 889–898.
[57] S. Engelmann, R.L. Bruce, F. Weilnboeck, G.S. Oehrlein, D. Nest, D.B. Graves, C. Andes, E.A. Hudson, Dependence of polymer surface roughening rate on deposited energy density during plasma processing, Plasma Process. Polym. 6 (8) (2009) 484–489.
[58] J. Robertson, Diamond-like amorphous carbon, Mater. Sci. Eng. R: Rep. 37 (4–6) (2002) 129–281.
[59] A.K. Shukla, R. Balasubramaniam, Effect of surface treatment on electrochemical behavior of CPTi, Ti-6Al-4V and Ti-13Nb-13Zr alloys in simulated human body fluid, Corros. Sci. 48 (7) (2006) 1696–1720.
[60] M. Bilek, D. McKenzie, A comprehensive model of stress generation and relief processes in thin films deposited with energetic ions, Surf. Coat. Technol. 200 (14–15) (2006) 4345–4354.
[61] G. Mallikarjunachari, P. Ghosh, Analysis of strength and response of polymer nano thin film interfaces applying nanoindentation and nanoscratch techniques, Polymer 90 (2016) 53–66.
[62] D. Rodriquez, J.G. Kohl, P. Morel, K. Burrows, G.G. Favaro, S.E. Root, J. Ramírez, M.A. Alkhadra, C.W. Carpenter, Z. Fei, Measurement of cohesion and adhesion of semiconducting polymers by scratch testing: effect of side-chain length and degree of polymerization, ACS Macro Lett. 7 (8) (2018) 1003–1009.
[63] H. Deng, T.W. Scharf, J.A. Barnard, Adhesion assessment of silicon carbide, carbon, and carbon nitride ultrathin overcoats by nanoscratch techniques, J. Appl. Phys. 81 (8) (1997) 5396–5398.
[64] S. Tajima, K. Komvopoulos, Effect of reactive species on surface crosslinking of plasma-treated polymers investigated by surface force microscopy, Appl. Phys. Lett. 89 (12) (2006) 124102.
[65] S. Bakshi, K. Balani, T. Laha, J. Tercero, A. Agarwal, The nanomechanical and nanoscratch properties of MWNT-reinforced ultrahigh-molecular-weight polyethylene coatings, JOM 59 (7) (2007) 50–53.
[66] D. Hegemann, Controlling the nanostructure and stability of a-C:H:N plasma polymers, Thin Solid Films 581 (2015) 2–6.
[67] T.R. Gengenbach, H.J. Griesser, Deposition conditions influence the postdeposition oxidation of methyl methacrylate plasma polymer films, J. Polym. Sci. A: Polym. Chem. 36 (6) (1998) 985–1000.
[68] D.E. Robinson, D.J. Buttle, J.D. Whittle, K.L. Parry, R.D. Short, D.A. Steele, The substrate and composition dependence of plasma polymer stability, Plasma Process. Polym. 7 (2) (2010) 102–106.
[69] S. Zanini, R. Ziano, C. Riccardi, Stable poly(acrylic acid) films from acrylic acid/argon plasmas: influence of the mixture composition and the reactor geometry on the thin films chemical structures, Plasma Chem. Plasma Process. 29 (6) (2009) 535–547.
[70] J. Ryssy, E. Prioste-Amaral, D.F. Assuncao, N. Rogers, G.T. Kirby, L.E. Smith, A. Michelmore, Chemical and physical processes in the retention of functional groups in plasma polymers studied by plasma phase mass spectroscopy, Phys. Chem. Chem. Phys. 18 (6) (2016) 4496–4504.
[71] S. Yu, Z.T. Yu, G. Wang, J.Y. Han, X.Q. Ma, M.S. Dargusch, Biocompatibility and osteoconduction of active porous calcium-phosphate films on a novel Ti-3Zr-2Sn-3Mo-25Nb biomedical alloy, Colloids Surf. B: Biointerfaces 85 (2) (2011) 103–115.
[72] A.W. Feinberg, P.W. Alford, H.W. Jin, C.M. Ripplinger, A.A. Werdich, S.P. Sheehy, A. Grosberg, K.K. Parker, Controlling the contractile strength of engineered cardiac muscle by hierarchal tissue architecture, Biomaterials 33 (23) (2012) 5732–5741.
[73] T.R. Gengenbach, H.J. Griesser, Aging of 1,3-diaminopropane plasma-deposited polymer films: mechanisms and reaction pathways, J. Polym. Sci. A: Polym. Chem. 37 (13) (1999) 2191–2206.
[74] E. Denisov, Cage effects in a polymer matrix, Macromol. Chem. Phys. 8 (S19841) (1984) 63–78.
[75] A. Gopferich, Mechanisms of polymer degradation and erosion, Biomaterials 17 (2) (1996) 103–114.
[76] K. Vasilev, L. Britcher, A. Casanal, H.J. Griesser, Solvent-induced porosity in ultrathin amine plasma polymer coatings, J. Phys. Chem. B 112 (35) (2008) 10915–10921.
[77] R. Toomey, D. Freidank, J. Ruhe, Swelling behavior of thin, surface-attached polymer networks, Macromolecules 37 (3) (2004) 882–887.
[78] B. Akhavan, B. Menges, R. Förch, Inhomogeneous growth of micrometer thick plasma polymerized films, Langmuir 32 (19) (2016) 4792–4799.
[79] J. Rodriguez-Hernandez, Wrinkled interfaces: taking advantage of surface instabilities to pattern polymer surfaces, Prog. Polym. Sci. 42 (2015) 1–41.
[80] R. Pankov, K.M. Yamada, Fibronectin at a glance, J. Cell Sci. 115 (20) (2002) 3861–3863.
[81] O.J.T. McCarty, Y. Zhao, N. Andrew, L.M. Machesky, D. Staunton, J. Frampton, S.P. Watson, Evaluation of the role of platelet integrins in fibronectin-dependent spreading and adhesion, J. Thromb. Haemost. 2 (10) (2004) 1823–1833.
[82] A.M. Moursi, C.H. Damsky, J. Lull, D. Zimmerman, S.B. Doty, S.I. Aota, R.K. Globus, Fibronectin regulates calvarial osteoblast differentiation, J. Cell Sci. 109 (1996) 1369–1380.
[83] R.K. Globus, S.B. Doty, J.C. Lull, E. Holmuhamedov, M.J. Humphries, C.H. Damsky, Fibronectin is a survival factor for differentiated osteoblasts, J. Cell Sci. 111 (1998) 1385–1393.
[84] A.M. Moursi, R.K. Globus, C.H. Damsky, Interactions between integrin receptors and fibronectin are required for calvarial osteoblast differentiation in vitro, J. Cell Sci. 110 (1997) 2187–2196.
[85] M. Heller, P.W. Kammerer, B. Al-Nawas, M.A. Luszpinski, R. Forch, J. Brieger, The effect of extracellular matrix proteins on the cellular response of HUVECS and HOBS after covalent immobilization onto titanium, J. Biomed. Mater. Res. A 103 (6) (2015) 2035–2044.
[86] E. Vanderleyden, S. Van Bael, Y.C. Chai, J.P. Kruth, J. Schrooten, P. Dubruel, Gelatin functionalised porous titanium alloy implants for orthopaedic applications, Mater. Sci. Eng. C: Mater. Biol. Appl. 42 (2014) 396–404.
[87] M. Hirota, H. Shimpo, C. Ohkubo, T. Umegaki, T. Toyama, T. Hayakawa, Bone adaptation of fibronectin-immobilized titanium implants using a tresyl chloride-activated method, J. Hard Tissue Biol. 24 (4) (2015) 341–345.
[88] E. Yoshida, Y. Yoshimura, M. Uo, M. Yoshinari, T. Hayakawa, Influence of nanometer smoothness and fibronectin immobilization of titanium surface on MC3T3-E1 cell behavior, J. Biomed. Mater. Res. A 100A (6) (2012) 1556–1564.

[89] C.D. Hodneland, Y.S. Lee, D.H. Min, M. Mrksich, Selective immobilization of proteins to self-assembled monolayers presenting active site-directed capture ligands, Proc. Natl. Acad. Sci. U. S. A. 99 (8) (2002) 5048–5052.
[90] L.S. Shlyakhtenko, A.A. Gall, J.J. Weimer, D.D. Hawn, Y.L. Lyubchenko, Atomic force microscopy imaging of DNA covalently immobilized on a functionalized mica substrate, Biophys. J. 77 (1) (1999) 568–576.
[91] M. Ronga, A. Fagetti, G. Canton, E. Paiusco, M.F. Surace, P. Cherubino, Clinical applications of growth factors in bone injuries: experience with BMPs, Injury 44 (2013) S34–S39.
[92] N.E. Epstein, Complications due to the use of BMP/INFUSE in spine surgery: the evidence continues to mount, Surg. Neurol. Int. 4 (Suppl 5) (2013) S343.
[93] K. Schmidt-Bleek, B.M. Willie, P. Schwabe, P. Seemann, G.N. Duda, BMPs in bone regeneration: less is more effective, a paradigm-shift, Cytokine Growth Factor Rev. 27 (2016) 141–148.
[94] Z. Gorgin Karaji, M. Speirs, S. Dadbakhsh, J.P. Kruth, H. Weinans, A.A. Zadpoor, S. Amin Yavari, Additively manufactured and surface biofunctionalized porous nitinol, ACS Appl. Mater. Interfaces 9 (2) (2017) 1293–1304.
[95] R.A. Latour, Perspectives on the simulation of protein–surface interactions using empirical force field methods, Colloids Surf. B: Biointerfaces 124 (2014) 25–37.
[96] T. Albrektsson, C. Johansson, Osteoinduction, osteoconduction and osseointegration, Eur. Spine J. 10 (2) (2001) S96–S101.
[97] M.J. Cooke, S.R. Phillips, D.S.H. Shah, D. Athey, J.H. Lakey, S.A. Przyborski, Enhanced cell attachment using a novel cell culture surface presenting functional domains from extracellular matrix proteins, Cytotechnology 56 (2) (2008) 71–79.
[98] Y.Z. Yang, R. Glover, J.L. Ong, Fibronectin adsorption on titanium surfaces and its effect on osteoblast precursor cell attachment, Colloids Surf. B: Biointerfaces 30 (4) (2003) 291–297.
[99] D.M. Rivera-Chacon, M. Alvarado-Velez, C.Y. Acevedo-Morantes, S.P. Singh, E. Gultepe, D. Nagesha, S. Sridhar, J.E. Ramirez-Vick, Fibronectin and vitronectin promote human fetal osteoblast cell attachment and proliferation on nanoporous titanium surfaces, J. Biomed. Nanotechnol. 9 (6) (2013) 1092–1097.
[100] S. Otsuru, K. Tamai, T. Yamazaki, H. Yoshikawa, Y. Kaneda, Circulating bone marrow-derived osteoblast progenitor cells are recruited to the bone-forming site by the CXCR4/stromal cell-derived factor-1 pathway, Stem Cells 26 (1) (2008) 223–234.
[101] H. Cheng, W. Jiang, F.M. Phillips, R.C. Haydon, Y. Peng, L. Zhou, H.H. Luu, N. An, B. Breyer, P. Vanichakarn, Osteogenic activity of the fourteen types of human bone morphogenetic proteins (BMPs), JBJS 85 (8) (2003) 1544–1552.
[102] J. Van der Stok, E.M. Van Lieshout, Y. El-Massoudi, G.H. Van Kralingen, P. Patka, Bone substitutes in the Netherlands – a systematic literature review, Acta Biomater. 7 (2) (2011) 739–750.
[103] V. Campana, G. Milano, E. Pagano, M. Barba, C. Cicione, G. Salonna, W. Lattanzi, G. Logroscino, Bone substitutes in orthopaedic surgery: from basic science to clinical practice, J. Mater. Sci.: Mater. Med. 25 (10) (2014) 2445–2461.
[104] A. Kadam, P.W. Millhouse, C.K. Kepler, K.E. Radcliff, M.G. Fehlings, M.E. Janssen, R.C. Sasso, J.J. Benedict, A.R. Vaccaro, Bone substitutes and expanders in spine surgery: a review of their fusion efficacies, Int. J. Spine Surg. 10 (2016) 33.